Referee number 1

Title: Aerosol concentration determines the height of warm rain and ice initiation in convective clouds over the Amazon basin.

Submitted: Braga
et al To: ACP
Date: March 30
2017 Decision:
Rejected

The structure is response after the quoted text of the reviewer.
The authors thank the referee for the general comments and advices. Furthermore, the advices of the referee are highly appreciated as well as the very valuable and constructive suggestions to increase the quality of the manuscript. We tried to address the points requested by the reviewer to the paper be considered for publication.

Summary:
This manuscript studies the effects of aerosol particle number concentration on the initiation of raindrops and ice hydrometeors in growing convective cumulus over the Amazon. Data from aerosol and cloud probes on board of the HALO aircraft are used. The values of the estimated *Na* at cloud base were applied to classify the atmospheric conditions where convective clouds developed as a function of aerosol particle number concentration (i.e., clean, polluted, and very polluted regions). Main conclusion was that cloud depth, assuming adiabatic assumptions) is related to aerosol characteristics at the surface.

A: The reviewer writes: "Main conclusion was that cloud depth, assuming adiabatic assumptions) is related to aerosol characteristics at the surface."
Where did the reviewer get such an idea from? We did not make or even hint to such a claim.

Major issues:

This paper claims that cloud depth and precip initiation are related to aerosol number concentrations at the cloud base.

A: We did not claim that depth is related to aerosol number concentrations at the cloud base.

We show that the height above cloud depth for rain initiation is related to cloud base drop concentrations.

I argue that precip formation in the clouds are related to saturation rate, updrafts and shear (turbulence), T gradients, stability, and particle type.

A: Indeed, precipitation initiation depends on saturation, which is determined by cloud base updraft and CCN. T gradient and shear determines the updraft and vertical extent of the cloud. Particle type is water drops. So where does the reviewer disagree with us?

I really do not like simplified convective clouds dependency on only aerosol concentration at the cloud base. Doing this you ignored non-adiabatic terms that include radiation, turbulence, and mixing can play important role for cloud structure.

A: We have shown in a series of papers referenced here why the adiabatic approximation to adiabatic r_e works. We also show the goodness of the simplified relationships. The disliking of the reviewer of this reality is not relevant to its validity.

In fact difference between the adiabatic ref and observed indicates that. There are several issues with figs such as averaging time, RWC but images do not show any, and Fig. 1b concept.

A: This comment is incomprehensible.

Why this work uses reff rather than use of full spectra for precip? Ref can be 12 micron but no droplets can be at that size range. Is this for a climate study or cloud study? Author should emphasize this.

A: This comment is incomprehensible.

Ref usually is almost constant above 3000 m in the plots but you show like exp curves.

A: The lines are the adiabatic r_e. This is stated very clearly.

You mention rain water content but none of the images is shown for rain droplets.

A: Images of rain drops are show in Figures 11a, 11b, 14a, 14b.

You are using different time segments for each case that is not acceptable (see figures top titles).

A: Which figures?

You need to show time series of ref, lwc, nd and ni for 2 cases (polluted and clean and pitch angle). Your physical values can be affected by aircraft INS system conditions.

A: We present here a higher level data for all cases. The raw data are available for anyone to inspect from the ACRIDICON archive.

Fig. 1b; shows a conceptual sketch but I feel that is not true. Droplets cant grow continuously to the cloud top level. Any work that reference the similar conditions cannot be considered for publication.

A: Before making such invalid statements so strongly, we recommend that the reviewer will read:

Beals, M. J., Fugal, J. P., Shaw, R. A., Lu, J., Spuler, S. M. and Stith, J. L.: Holographic measurements of inhomogeneous cloud mixing at the centimeter scale, Science, 350(6256), 87–90, doi:10.1126/science.aab0751, 2015.

Major issues can be listed as

1. DWC=0.01 g m-3 used for DWC to get rain out of the cloud. What this is selected not clear. DWC can be 0.01 g m-3 but 5 droplets ot 100 of droplets. I argue that this is not

an acceptable assumption for cloud structure?

A: The reviewer writes that the threshold is "to get rain out of the cloud". This is not what we wrote. This threshold is used for in situ rain initiation. We wrote that "DWC, defined here as the mass of the drops integrated over the diameter range of 75–250 μm (Freud and Rosenfeld, 2012)". The reason for limiting the maximum drop size to 250 μm is because it has a terminal fall velocity of 1 m/s. This minimizes the chance that the rain fell from above and not initiated near the penetration height.

2. You say that rain occurred at higher levels in more polluted clouds; no RH profile is shown or icing detector (pg 10) ; how do you know the cloud structure and particle phase? In fact none of your figures show rain or cloud droplets at larger sizes.

A: Images of rain drops are show in Figures 11a, 11b, 14a, 14b. RH is irrelevant within the cloud. Why should we use icing detector while we have liquid water content and temperature, thereby quantifying supercooled liquid water content? Cloud phase is known by the hot wire liquid water content and CIP images.

3. Figure 1b; this figure really mean nothing for me, and doesn't help anything about understanding of cloud macro structure. We know that aerosols can play significant role in cloud development, specifically for stratiform clouds. Below the cloud base aerosols act as nuclei, and they are activated within the cloud base, then dynamics of the system play a role faster that diffusional growth of particles. Certainly mixing happens at the base and edges of the system. Conditions are not adiabatic clearly. In fact if saturation is high enough and lots of moisture exist, many droplets forms. Do you show any vertical profile of the cloud T, w, and qv? In fact when cloud top increases at the upper troposphere not many particle reach to cloud top. Therefore, cloud depth is not only function of Na but vertical air velocity which is lowest at the cloud top at the upper troposphere. In fact because of collision/coalescence/aggregation processes, many particles fall down as precip before reaching the cloud top. Therefore, I will not accept your claims here for your work.

A: The captions of Figure 1b read: "Flight patterns below and in convective clouds during the ACRIDICON-CHUVA campaign".

The title of the paper reads: "Aerosol concentrations determine the height of warm rain and ice initiation in convective clouds over the Amazon basin".
It should have been very clear to the reviewer that our study focuses in the lower parts of the clouds between cloud base and height of precipitation initiation. All the objections of the reviewer pertain to processes that affect cloud microstructure and precipitation above the height of precipitation initiation.

4. Fig.2; most of ref is between 11-14 micron for precip occurrence>50%; then how accurate to use ref as a precip condition. Precip is function of Nd, Vt, wa, and shape. Differences of these parameters at various T, can affect reff strongly. Suggests that cloud depth is not only function of Na but other physical and dynamical para,eters.

A: Indeed, cloud depth is not a function of N_a, and we never made such a strange claim.

5; I like to see time series of Nd, Ni, RH, and ref for clean and clean cases. Use of reff for a cloud microphysics case study may not be appropriate. Ref can be 15 micron with no rain or with rain depends on psd.

A: How is this comment relevant to the subject of the study?

6; fig 4 may not be needed, this is well
known.

A: Its validity has to be demonstrated to the subject clouds.

7; figure 5;
I like to see time series of Nd, showing about 2000 cm-3, also Na, please provide.

A: We don't see what will the time series of N_d would add to the points made in this study? We have too many figures already.

This figure shows that Nd is constant above 0C, and increases to warmer T. To me this is an artifact. Please also show LWC time series. Also show the weighted line on the plot.

A: We don't agree. Figure 5 shows clearly a steady decrease of N_d with height.

Fig. 6a; thi is shown for 25 sec but others are for 656 sec, please be consistent.

A: At cloud base we have much more sampling than at the narrow towers aloft. We took all the samples that we could get with the aircraft.

Fig6b; looks like no changes in reff are for T<0C. For a given T difference is about 2-3 micron; it means that uncertainty in reff can be up to 3 micron, then how can someone use your method for cloud depth.

A: The reviewer repeats his misconception about what we do in this paper.

Fig. 7a; Combination of cip and cdp? Based on image shown, there are cloud droplets, CIP doesn't show anything.

A: The images are made by the CIP. Indeed, the CIP shows only cloud droplets.

Fig 7b; doesn't show droplets or drizzle? Where is the rain water come from?

A: All CIP images are converted as if they were rain.

Fig 7c; same again where is the RWC come from? Image shows ice crystals or rimed particles.

A: See response to the previous comment.

Fig. 9; again for Dc>3000 m, re is constant. This shows that re-Dc relationship doesn't hold.

A: We don't agree. r_e increases up to D_c=4500 m. At that height ice forms on expense of the cloud droplets, as shown in Figure 18.

Fig. 10a; Nd is constant within the cloud, looks like well mixed layer. Then how ref increases with depth? Flight is only 3 mins? Looks like ref increases with LWC. Can you show reff versus LWC?

A: The lack of decrease of N_d with height could be related to some secondary droplet nucleation, as indicated in Figure 11a.

Fig 11a; assumed that drizzle has sizes >50 micron why we don't have RWC? Or precip? Again image shows ice crystals, not drizzle.

A: The image shows nice rounded rain drops. It even shows one pair of drops while coalescing!

Fig. 11b; image shows graupel, where is the rain coming from, you say 0.27 g m-3?

A: The image shows large rounded rain drops. It even shows one pair of drops while coalescing!

Fig. 12:

I really have issues with this figure. If you look at the lines for a given Na say 1 or 100; and then check the Da. Not easy to make any conclusion based on this figure. In fact any uncertainty for less than about 20 cm-3 can results no discrimination among these cases.

A: The figure clearly shows that while total PCASP in AC12 is 10 times the PCASP in AC19, concentrations of particles > 2 □m are 5 time larger in AC19 compared to AC12.

Fig 13; same as before. How do you know they are droplets?

A: The CDP is rather insensitive to ice particles, and the hot wire LWC was similar to the CDP LWC.

13a; again like rimed particles. RWC=0 but you show only 5 sec spectra, you are not consistent with time averages.

A: The reviewer probably means Figure 14a. We take the sample size that we can get under these challenging flight conditions.

13b; again not rain water but mostly they are graupel or rimed particles. Only 4 second average? Not consistent. If CWC=0.247 and RWC=0.27 and DWC=0.16, then rain amount is more than cloud water content? How do you explain this over 4 sec?

A: Again, we take what we can get. At this height most cloud water was converted to precipitation.

Fig. 16; why there is no RWC? You have particles more than 100 micron but not rain?

A: See the CIP precipitation images.

Fig. 17; Dc versus Na relationship can't be a linear relationship. Increasing aerosols doesnt result in larger Dc values. Other factors should be considered e.g. updrafts, stability, diabatic heating etc.

A: These are our results, whether we like it or not, and whether it support or contradicts our concepts. We refer the reviewer to read: the paper which we reference in this context:

Freud, E. and Rosenfeld, D.: Linear relation between convective cloud drop number concentration and depth for rain initiation, J. Geophys. Res. Atmos., 117(2), 1–13, doi:10.1029/2011JD016457, 2012.

Fig. 18; as noted previously above 3000 m, ref is almost constant but here you show all DC values increase with increasing ref exponentially. This figure should be discussed based on my previous points.

A: The figure caption states that the lines are the adiabatic cloud drop effective radius (r_{ea}).

Other point I am not comfortable is that almost largest WC is at the cloud top which cant be correct. This is function of Vf, and you never mentioned this.

A:We don't agree strongly with the reviewer, for reasons that we explained in a previous response.

Discussion section should focus on the uncertainty of the observations and method. Presently it is not focusing on observations/analysis uncertainties such as averaging over various time segments.

A: The averaging over various time segments is part of the analysis.

Conclusion section should have clear findings that are related to observations collected from the field project. It can be good idea to list them.

A: The findings will be listed in the new version.

Minor points are not considered in this point.

Interactive response to reviewer's comment on "Aerosol concentrations determine the height of warm rain and ice initiation in convective clouds over the Amazon basin" by Ramon Campos Braga et al. Anonymous Referee #2

The structure is response after the quoted text of the reviewer.

The authors thank the referee for the general comments and advices. Furthermore, the advices of the referee are highly appreciated as well as the very valuable and constructive suggestions to increase the quality of the manuscript. We tried to address the points requested by the reviewer to the paper be considered for publication.

Reviewer's text:

A strength of this paper is the presentation of cloud in-situ observations that addresses the question of how convective clouds are influenced by changing the concentration of aerosols. The authors have determined that the height of rain initiation given by D_i is approximately 5 * the number concentration of cloud droplets at cloud base, N_d. This type of study is needed for developing parametrisations. It is difficult to obtain such a wide range of values of N_d using a single location for the study.

There are a number of problems with the paper however.

1. There are no details about the environment of the clouds, the effect of different cloud bases, or the dynamics and history of the clouds. For example, there should be information for each cloud pass about the distance from cloud top, the horizontal distribution along the track of the vertical wind and the location where different measurements were made. Also, it is important to know the history of the cloud before that pass. Does the cloud and the aircraft indeed follow the pattern illustrated in Fig 2? None of the diagrams in Supplementary Fig 1 seem similar to Fig 1b. An example is Figs. 7b-c and 8. How far was the pass below the cloud top? Supercooled raindrops would only be observed in the updraft region.

A: As we mentioned in the manuscript, convective clouds develop as clusters. During the flights, the flight scientist found a region with growing convective cumulus with different stages of development from very shallow to very deep clouds. The cloud passes occurred near the tops of growing convective cumulus were performed about 100-300 m below cloud top, as estimated by the flight scientist, assisted by the pilots (we already highlighted these details while describing Figure 1 at Introduction section). Figure 1 is highly schematic and illustrates the ideas that we measured successively higher clouds near their tops in the same cloud cluster. This type of cloud profile flight was adopted because it provides the closest information as possible about cloud particles formation as a function of cloud depth near the top of growing convective towers. In addition, this type of flight is the safest because the pilots could see the end of the cloud, avoiding the risk of penetrating the cores of Cb.

The details about cloud base temperature and heights are available at Table 3. The details about the location of measurements (Figures 1) and vertical velocities (Figures 3) are available at supplementary material.

2. Are there multiple thermals? These can be important for the development of raindrops?

A: No cloud is composed of a single thermal. But the question of multiple thermal is relevant for rain formation only if raindrop that was formed above the cloud penetration level was recirculated to the penetration level. Since we were fairly close to cloud tops, this was not an issue.

3. Turbulence enhancement of collision and coalescence and the enhancement of droplet growth due to entrainment and mixing are not considered in the analysis. Both of these processes would change the simple relationship between D_i and N_d. Giant and ultra-giant aerosols are mentioned, but likewise the analysis does not consider them carefully.

A: The effects of turbulence are inherently fully taken into account in the observed cloud properties, whether we acknowledge it or not.

Cloud drop size distribution did not show a separate large mode below the height where cloud drop effective radius > 14 µm, where coalescence leads to fast rain initiation. This means that GCCN did not have a major impact on rain initiation. In any case, as for the turbulence, the reported relationships account for the occurrence of GCCN whether we acknowledge it or not.

4. The initiation of ice particles in convective clouds is complicated. The analysis presented does not discuss the critical aspects of the problem.

A: We just show what we observe. We have insufficient information to go beyond that for ice initiation.

5. The paper is poorly constructed. The font is far too small and diagrams used in discussions are in different documents. Also there are too many similar figures that show very little and are not properly discussed, while more detailed analysis and accompanying figures are missing.

A: The font used is the required by ACP. We have chosen show many figures at supplementary material to provide the opportunity to the reader check our findings.

Specific comments.

1. Abstract. "Rain initiation" is a loose term. The authors should be more precise."Initiated as ice hydrometeors". The word "initiated" is confusing.

A: Rain initiation is a commonly used term.
With respect to ice, the text was changed to: "the first observed precipitation particles were ice hydrometeors".

Does "polluted conditions" include biomass burning?

A: Yes.

Say why smaller cloud droplets froze at lower temperatures compared to the larger [cloud?] droplets in the [un - or less?] polluted cases. And give the sizes.

A: Smaller droplets are less likely to contain immersion freezing ice nuclei due to their lower volume, and are also less likely to meet contact ice nuclei due to their lower surface area. Smaller droplets are also less likely to incur ice multiplication processes.
The effective radius of cloud droplets (r_e) which freezes at -9.1 ºC was ~ 11.5 µm for flight AC07, while for flight AC13 r_e was ~10.2 µm at -14.1 ºC. Both flights were performed in polluted conditions over the deforestation arc at Amazon were similar type of aerosols are found (mostly from biomass burning).

"Entrainment and mixing almost completely inhomogeneous". It is the mixing that is either homogeneous or inhomogeneous. A value of r_e close to the r_ea value is not sufficient information to conclude that the mixing process is inhomogeneous. There could be only dilution and no evaporation.

A: The mixing is nearly inhomogeneous.

"Secondary nucleation". It's not true that this process will necessarily inhibit the formation of rain, and may indeed enhance it by providing more small droplets for collisions. Secondary nucleation does not mean that the larger cloud droplets are absent necessarily. Addition of more smaller droplets shifts the value of r_e to smaller sizes.

A: The text says:
"Secondary nucleation of droplets on aerosol particles from biomass burning and air pollution reduced r_e below r_{ea}, which **further inhibited** the formation of raindrops and ice particles and resulted in even higher altitudes for rain and ice initiation."
Secondary nucleation slows down the growth with height of the primary nucleated drops at cloud base. Therefore, we support that secondary nucleation prevent the formation of raindrops and ice particles before the first raindrop/ice starts to form. Once new droplets are nucleated above cloud base, the condensational growth rate of the cloud droplets

decreases due to the larger competition for the water vapor available. Then, the resulting cloud droplets take more time (requiring thicker cloud depths) to reach larger sizes via condensation process and initiate coagulation or freezing.

2. p2, lines 87-90. It is incorrect to assume that the mixing processes is completely inhomogeneous. And if it was, the vertical profile of the cloud drop effective radius would most likely not follow an idealized adiabatic parcel; there would be broadening.

A: The deviations from complete inhomogeneous mixing explain the deviations shown in many of the figures between the adiabatic and actual r_e. This is why we claim it is near inhomogeneous, but not ideally so.

3. Line 95. I am not in favour of the wording "raindrops start to form" or "rain initiation" (discussed throughout the paper) since it is a stochastic process.

A: Indeed everything is stochastic, but since the formation rate of raindrops is proportional to the 5^{th} power of r_e, and r_e increases with height, it is quite OK to mention height for rain initiation in practical terms. This is what this paper is about.

4. p3, lines 112-113. See #2 above, and furthermore, the vertical values of r_e would not necessarily be constrained by N_d at cloud base.

A: The previous studies cited here support these characteristics for convective clouds.

5. p3, line 138. Downdrafts can be significant. This is a good reason why the vertical velocity time series and the distance below cloud top should be shown.

A: The reason for limiting the maximum drop size to 250 µm for drizzle water content calculation was because it has a terminal fall velocity of up to 1 m/s. As convective clouds are a turbulent medium large updrafts and downdrafts than 1 m/s were found (this is shown at Figures 3 in supplementary material). Again, this is just an extra measure of caution on top of measuring clouds near their tops, where nothing can come from much greater heights.

6. p6, line 238. What was the wind direction and where were the clouds relative to the opening of the river in Fig1a?

A: The wind direction was east-north-easterly. See the location of the flight in clouds in Figure 1, at the northeastern most edge of the flight track.

7. p8, line 329. Is it possible to show the CDP size distribution just below cloud base?

A: Yes. We show in the revised version of the manuscript (Figure 12) the mean total number concentration calculated with PCASP and CCP-CDP for ~200 s of measurements below cloud base during the flights AC12, AC18 and AC19 . The flight AC19 over the Atlantic Ocean (where we indicate the possibility of GCCN) presents higher concentration of particles > 1 µm. This is observed with PCASP and CCP-CDP. The mean total number concentration of large particles measured with CCP-CDP over the ocean is about 10 times greater than observed inland. These values highlight the difference between the size of aerosol which can activate as cloud droplet over the ocean and over Amazon basin.

8. p8, lines 339-340. The adiabatic parcel model would presumably use the aerosol size distribution, including the giant ccn, to initiate the cloud drops.

A: We merely calculated the adiabatic water content and divided by cloud base drop concentrations to obtain adiabatic r_v. The r_e was calculated by r_e=1.08 r_v.

9. p8, line 344. Electrification is not part of this paper. This statement is conjecture.

A: The text was changed from "the low remaining amount of cloud water suppresses the development of cloud electrification" to "the low remaining amount of cloud water reduced a key ingredient for cloud electrification".

10. p8, lines 345-346. It is not evident that downdrafts commence after rain starts. More detailed analysis is needed.

A: Observed downdrafts starts to be evident or more intense above 1660 m after rain starts for flight AC19. Above 1660 m, more downdrafts than updrafts were observed.

11. p8, lines 346-349. The sentence does not make sense.

A: The sentence was rewritten as follows:
"The values of vertical velocities measured at flight AC19 (clean region) were smaller than measured for flight AC07 (very polluted region). However, for both cases updrafts are more evident during droplets growth via condensation and downdrafts are most notable when precipitation particles are observed in the cloud."

12. p8, lines 349-350. More evidence is required. The stronger updraft in Fig 3a of the supplement could be due to environmental conditions.

A: We cannot exclude the enhancement of the updrafts due to environmental conditions.
New text:
"Strong updrafts (~10 m s^{-1}) are observed in polluted cases after ice starts to form, probably due to the latent heat release during freezing processes. An alternative explanation of updraft enhancement due to environmental conditions in these cases cannot be excluded."

13. p9, line 358. There should be more discussion of Figs 13 and 14. Also, again, the images and size distributions should be presented in the context of the updraft structure. For example, the larger particle in the top panel of Fig 14a looks like a graupel particle. Has particle recognition been performed?

A: The CCP-CIP images were used to distinguish raindrops and ice particles during cloud passes. The hydrometeor type is identified visually by their shapes. The phase of the smaller CCP-CIP particles cannot be distinguished. We believe that at Fig14a we have not graupel particle but some raindrops. The general characteristics of vertical velocities were discussed already in the paper.

14. p9, line 360. As above, it is not right to have some of the figures used in the arguments in the supplementary material and others included in the paper. The diagrams are used in the same way as figures in the manuscript. The authors make a strong statement in the paper based on two cases with one of them shown in the supplementary material.

A: We just highlight what we found. We have already many figures in the paper and some of them we had to send for supplementary material because of editorial objections. We present here this question to the co-editor.

15. p9, line 360 Change the last word in the line (this) to "the" since Fig 5S shows plots constructed for two levels.

A: OK. Thanks.

16. What is the evidence that the images in Fig 5aS are spherical? Some of the larger particles in Fig 5bS do look spherical, but it is not possible to tell for the smaller particles.

A: Indeed, this is why we claim the rain/ice initiation to the larger particles. As we mention before we could not recognize the phase of particles, but only their shapes for precipitable ones.

17. And now back to Fig 14b... Representative images from all parts of the cloud pass should be shown in all cases. What is the difference between almost spherical particles in

Fig 14b and the same in Fig5S?

A: Image 14b shows the first pass in which ice hydrometeors are observed mixed with supercooled rain drops. Rain drops were observed also at lower levels, as summarized in Figure 18.

Figure 5S shows that in AC18 first rain drops are observed at the -5.7 C isotherm, and that they still remain liquid, or at least spherical, at the -11.4 C isotherm.

18. p9, lines 364 to 371. There is no discussion about the effect of the difference in cloud-base temperature. The main problem with the discussion, however, is there is no mention of the effects of inhomogeneous mixing, or even the decrease in N observed in the two flights: e.g. N_max at 10 deg is the same (500/cc) in AC18 (Fig 4aS) as in AC09 (Fig 13a).

A: The inhomogeneous mixing is implicit when r_e is closer to r_{ea} by the reasons that we mentioned before. At the same temperature Nmax can be the same, but r_e is larger for AC09, because the 10 C isotherm is higher above cloud base in AC09 compared to AC18.

19. p9, lines 371-374. It is not clear what is meant by the association with vertical velocities? The rate of condensational growth does not depend on vertical velocity.

A: The sentence was removed.

20. p9, lines 382 - 384. It is not a relative increase. It is perhaps more surprising that there is such a decrease in N_max between the lowest and next level in AC07 (Fig 5). More analysis should be shown to support suggestions made about secondary activation.

A: We don't assert that it is due to secondary activation. We just raise the possibility.

21. p9, lines 387 - 388. Should it not be the reduced rate of production of raindrops due to lower collision and coalescence efficiencies? There is no process of inhibition or suppression in the cloud.

A: The text was modified to: "These results highlight the role of aerosols in inhibition of raindrop formation due to inducing a larger N_d and respective lower r_e, which leads to suppression of collision and coalescence processes in very polluted regions."

22. p9, lines 388 - 389. 300 m is not a great distance when making aircraft passes. Is the result significant? What is the explanation?

A: Indeed, it is not a significant difference, but nevertheless in the right direction, this is worth noting.

23. p10, lines 393 - 394. As with so many other statements in the paper, more analysis should be presented to support the statement. What is the variation of CCN and updraft speeds at cloud base, for example?

A: The acceleration of updrafts above the height of cloud base increases supersaturation and thus can induce secondary drop activation. For flights which we observed the increase of N_d with height, high aerosol concentration was observed indicating increased likelihood of secondary nucleation of droplets above cloud base.

24. I believe the discussion and conclusions should be edited based on the referee comments.

A: The conclusions did not change.

Interactive response to reviewer's comment on "Aerosol concentrations determine the height of warm rain and ice initiation in convective clouds over the Amazon basin" by Ramon Campos Braga et al.

The structure is response after the quoted text of the reviewer.

The authors thank Darrel Baumgardner for the general comments and advices. Furthermore, the advices of the referee are highly appreciated as well as the very valuable and constructive suggestions to increase the quality of the manuscript. We tried to address the points requested by the reviewer to the paper be considered for publication.

Reviewer's text:

The authors have presented the case that cloud active aerosols at cloud base are responsible for determining the cloud depth at which precipitation forms. As pointed out in the introduction, this is not a new discovery and has been investigated in many regions by many researchers other than the ones that are heavily referenced in this paper. Although the failure to be more inclusive in mentioning these other studies is not a fatal flaw in this paper, it does weaken its overall premise and conclusions. There are more serious issues that I would like addressed before this study is published.

A: Four references to rain initiation were added.

Instrument issues

I could not find in either this paper or the Braga et al (2016) sufficient discussion on the processing of spectrometer measurements. In particular:

1) Coincidence corrections. Lance (2012) clearly shows that the CDP (unmodified with secondary mask) and CAS seriously undercount at > 500 cm-3. Lance (2012) says

nothing about interarrival times and coincidence. Interarrival is used for shattering, so I don't understand the justification for not correcting the concentrations. Many of the concentrations reported > 1000 cm-3 will likely be at least 50% larger which will seriously impact the derived LWC and subsequent Na.

A: Both instruments have different set ups compared to the configuration described in Lance et al. Specifically for the CAS, the pin hole in front of the sizing detector was changed to a smaller diameter. This significantly reduced the number of coincident particles. The analysis addressing coincidence was done following the paper by Lance (2012). We compared the LWC from the hotwire and the PSDs assuming spherical particles. If coincidence occurs in the sampling volume, larger but fewer particles would have been detected, thus the LWC from the particle probes would be higher for higher number concentrations. The CAS showed rather lower LWC than the hotwire at higher number concentrations (> 1000 cm-3), which stands in contrast to the observations by Lance et al.

Furthermore, we looked at the Poissonian probability density function of the inter arrival times at high number concentrations (2000 cm-3). If coincidence occurs then a significant fraction of the inter arrival times should be at the lower end of the distribution (short inter arrival times) or even beyond the time resolution of the instrument. We could not find a significant fraction (< 5 %) at the lower end of the inter arrival time distribution.

The CDP additionally measures the transit time. The transit time did not increase (unlike like the CDP in Lance et al. did) with the number of particles detected up to number concentrations of 1500 cm-3.

Further, the good agreement of CAS and CDP regarding the number concentrations shows, if coincidence was an issue, it would be of similar magnitude for both instruments, which is very unlikely.

The three independent analysis methods in addition to the good comparison of the probes proves that there are no indications of coincidence in our measurements.

2) In the images from the CIP, there are many out of focus droplets (donuts). The Korolev (2007) correction has to be done, otherwise the derived water content will be an

overestimate and the height of precipitation might be incorrect.

A: For the data processing of the CCP measurements, ice was assumed as the predominant particle phase in the mixed-state cloud conditions that were mainly given throughout the ACRIDICON CHUVA campaign.

The ice assumption causes all images of droplets and ice particles to be treated and considered as particles (apart from shattering-induced particles) but the Poisson spot correction is then excluded.

The Korolev correction is defined for liquid drops only and the SODA image processing disables this correction process once the ice-phase is selected.

The assumption of ice density instead of water density implies a slight overestimation (~10 %) of the calculated rain water content for particles greater than 75 µm. This will be highlighted in the manuscript.

3) Was the PCASP operated with a heated inlet? If so, corrections are needed to size distribution.

A: No. PCASP was not operated with a heated inlet. We add a comment about this in the instrument description.

4) A fair amount of the paper is devoted to illustrating that the CAS and CDP compare within expected uncertainties. Given that this has already been done in the Braga et al. (2016), this is redundant and doesn't add much new information to the results.

A: We did not compare effective radius (r_e) calculated with CAS-DPOL and CCP-CDP as a function of mean volume radius and precipitation probability for at Braga et al. (2016). The results show that even with agreement the threshold of r_e for rain initiation is about 1 µm smaller for CAS-DPOL in comparison with CCP-CDP.

Science Issues

5) Modify title please. The current title is misleading and not correct. It currently implies

that all aerosols determine the depth of precipitation initiation. The results do not support this strong of a statement. Some types of aerosols play a role in determining the height of warm rain initiation, i.e. CCN/IN and their concentration have an impact as is clearly shown in this paper. A more accurate title might be "Further evidence for the impact of cloud base CCN/IN on the height of precipitation initiation"

A: We have changed the title to:

Further evidence for CCN aerosol concentrations determining the height of warm rain and ice initiation in convective clouds over the Amazon basin

6) The determination of Na needs much more explanation. The Na vs Precipitation depth is key to the conclusions and needs amplification. Why should the slope of the LWC vs Mv relationship with height provide a good estimate of Na? I understand that LWC = Nd*Mv but this is not discussed, nor is how Mv is derived. In addition, all the plots that determine Na should be shown. If they are anything like the one shown in Braga et al 2016, Fig. 14a, there can be a very large spread in values of LWC at each Mv and subsequent uncertainty in the Rea. Fig. 15 in Braga et al (2016) clearly show that there is a lot of dispersion when comparing Na and Nd. The best fit line in their Fig. 14a does not appear to fit the points and certainly can't justify reporting Na to such precision.

A: The reviewer wrote: "I understand that LWC = Nd*Mv". This is not quite so. The right expression is LWCa = Nda*Mva, where all are the adiabatic values. The whole idea of the methodology is that the actual r_e is similar to r_{ea} - the adiabatic effective radius, due to the nearly inhomogeneous nature of the mixing. The mixing does decorrelate LWC strongly from LWCa, while keeping r_e well correlated with r_{ea}.

The methodology which use LWC vs. Mv relationship with height to estimate *Na* is well tested and validated at Freud and Rosenfeld (2011). The *Na* estimate is also explained and tested at Braga et al. (2016). Indeed there are uncertainties related to Na estimated mostly related when secondary nucleation takes place. The model does not predict that Nd increases with height, but decrease due to coalescence and inhomogeneous cloud mixing.

The results suggest the occurrence of secondary activation with different strengths during flights AC08, AC12, AC13 and AC20 (see figures attached). Large updrafts were measured above cloud base during these flights which increase supersaturation inducing secondary activation. The increase of N_d with height was observed mostly when large aerosol amount was measured with PCASP and UHSAS above cloud base height. However, the estimation of N_a have shown to be useful to discriminate clean from polluted environments and predict the height for rain initiation.

7) Nothing is said about the uncertainty in the determination of level of precipitation wrt to vertical motions and where the precipitation actually initiated, i.e. it could have actually been below the level of measurement before being lofted upwards. This uncertainty can be estimated using the measured vertical motions.

A: Doing that would require information that we don't have about the rate of rain formation with height, and will constitute a circular argumentation. The scatter in Figure 17 is the best that we can do for illustrating the uncertainty.

8) Nothing is said about the time it takes to make the measurements at the various cloud levels and how these levels were selected. This will give some idea of the time during which the cloud is growing an how long it took to initiate precipitation.

A: Since the measurements were not following individual growing cloud towers, these times would not advance such knowledge.

9) Secondary nucleation is a very poor term because in a classical parcel model in an updraft, new particle nucleation occurs above cloud base until there are no more cloud active CCN at the level of SS. The implication here is that new CCN are being entrained and that is why the Nd increases with altititude, but this is likely not the case. When running a parcel model with a prescribed updraft and CCN spectra, the supersaturation increases in altitude as the parcel rises adiabatically and cools. The CCN will activate depending on their SS spectra and the available water. This needs revising.

A: The secondary CCN activation was observed mainly in cloud segments with updrafts that were much stronger than at cloud base. This supports the narrow definition of secondary activation as defined by the reviewer. However, we do not exclude the possibility of additional CCN being entrained and activated above cloud base.

10) The relationship Dr = 5*Na needs revising to take into account the data processing and uncertainties that I raise above, and needs an error bar.

A: The uncertainty of N_a calculation with CDP (14 %) is now included in the linear relationship. The linear relationship including N_a uncertainty is $D_r = (5 \pm 0.7) \cdot Na$.

Further evidence for CCN aerosol concentrations determining the height of warm rain and ice initiation in convective clouds over the Amazon basin

Ramon Campos Braga[1], *Daniel Rosenfeld*[2], *Ralf Weigel*[3], *Tina Jurkat*[4], *Meinrat O. Andreae*[5,9], *Manfred Wendisch*[6], *Ulrich Pöschl*[5], *Christiane Voigt*[3,4], *Christoph Mahnke*[3,8], *Stephan Borrmann*[3,8], *Rachel I. Albrecht*[7], *Sergej Molleker*[8], *Daniel A. Vila*[1], *Luiz A. T. Machado*[1], *and Lucas Grulich*[10]

[1] Centro de Previsão de Tempo e Estudos Climáticos, Instituto Nacional de Pesquisas Espaciais, Cachoeira Paulista, Brasil

[2] Institute of Earth Sciences, The Hebrew University of Jerusalem, Israel

[3] Institut für Physik der Atmosphäre, Johannes Gutenberg-Universität, Mainz, Germany

[4] Institut für Physik der Atmosphäre, Deutsches Zentrum für Luft- und Raumfahrt (DLR), Oberpfaffenhofen, Germany

[5] Multiphase Chemistry and Biogeochemistry Departments, Max Planck Institute for Chemistry, 55020 Mainz, Germany.

[6] Leipziger Institut für Meteorologie (LIM), Universität Leipzig, Stephanstr. 3, 04103 Leipzig, Deutschland

[7] Instituto de Astronomia, Geofísica e Ciências Atmosféricas, Universidade de São Paulo, Sao Paulo, Brazil

[8] Particle Chemistry Department, Max Planck Institute for Chemistry, 55020 Mainz, Germany.

[9] Scripps Institution of Oceanography, University of California San Diego, La Jolla, CA 92098, USA

[10] Institut für Informatik, Johannes Gutenberg-Universität, Mainz, Germany

Correspondence to: Ramon C. Braga (ramonbraga87@gmail.com)

Abstract: We have investigated how pollution aerosols affect the height above cloud base of rain and ice hydrometeor initiation and the subsequent vertical evolution of cloud droplet size and number concentrations in growing convective cumulus. For this purpose we used in-situ data of hydrometeor size distributions measured with instruments mounted on HALO (High Altitude and Long Range Research Aircraft) during the ACRIDICON-CHUVA campaign over the Amazon during September 2014. The results show that the height of rain initiation by collision and coalescence processes (D_r, in units of meters above cloud base) is linearly correlated with the number concentration of droplets (N_d in cm^{-3}) nucleated at cloud base ($D_r \approx 5 \cdot N_d$). When N_d exceeded values of about 1000 cm^{-3}, D_r became greater than 5000 m, and the first observed precipitation particles were ice hydrometeors. Therefore, no liquid water raindrops were observed within growing convective cumulus during polluted conditions. Furthermore, also the formation of ice particles took place at higher altitudes in the clouds in polluted conditions, because the resulting smaller cloud droplets froze at colder temperatures compared to the larger drops in the unpolluted cases. The measured vertical profiles of droplet effective radius (r_e) were close to those estimated by assuming adiabatic conditions (r_{ea}), supporting the hypothesis that the entrainment and mixing of air into convective clouds is nearly inhomogeneous. Secondary activation of droplets on aerosol particles from biomass burning and air pollution reduced r_e below r_{ea}, which further inhibited the formation of raindrops and ice particles and resulted in even higher altitudes for rain and ice initiation.

1. Introduction

Understanding cloud and precipitation forming processes and their impacts on the global energy budget and water cycle is crucial for meteorological modeling. Therefore, many studies have focused on improving cloud parameterization in numerical weather and climate models (e.g., Frey et al., 2011; Khain et al., 2005, 2000; Klein et al., 2009; Lee et al., 2007; Machado et al., 2014). These parameterizations need to represent in simplified form the complex chain of events that occur in clouds.

Cloud droplets form when humid air rises and becomes supersaturated with respect to liquid water. Then water vapor condenses onto surfaces provided by pre-existing cloud condensation nuclei (CCN, a list of abbreviations and symbols is given in Table 1) aerosols. For ice formation, the ambient temperatures must reach values lower than 0 °C. At temperatures between 0 ºC and -36 ºC, ice in convective clouds mostly forms inhomogeneously on ice nuclei (IN) aerosols, often when they interact with supercooled liquid water droplets (Pruppacher et al., 1998). At colder temperatures (less than -36 ºC), cloud particles freeze due to homogeneous ice nucleation (Rosenfeld and Woodley, 2000).

A cloud predominantly consists of droplets with diameters larger than about 3 µm, except for transient smaller sizes right at cloud base. The number concentration of cloud droplets (N_d in cm^{-3}) at cloud base mainly depends on the conditions below cloud base, i.e., the updraft wind speed (W) and the supersaturation (S) activation spectra of cloud condensation nuclei [$CCN(S)$] (Twomey, 1959). In very clean conditions, values of N_d near cloud base are in the range of ~50-100 cm^{-3}, while in polluted condition N_d may reach values between 1000-2000 cm^{-3} (Andreae, 2009; Rosenfeld et al., 2008, 2014a).

Below the freezing level, raindrops are formed due to cloud droplet coagulation (collision-coalescence) processes (warm rain process). Mixed phase precipitation results from interactions between ice particles and liquid water droplets (Pruppacher et al., 1998). Several studies based on aircraft, radar and satellite measurements support that warm rain formation requires that the cloud consists of droplets with values of the effective radius (r_e) larger than 13-14 µm (Freud and Rosenfeld, 2012; Konwar et al., 2012; Prabha et al., 2011; Chen et al., 2008; VanZanten et al., 2005; Pinsky and Khain, 2002; Gerber, 1996; Rosenfeld and Gutman, 1994).

The effects of aerosol particles on clouds and precipitation have been studied in different parts of the globe (e.g., Fan et al., 2014; Li et al., 2011; Ramanathan et al., 2001; Rosenfeld and Woodley, 2000; Rosenfeld et al., 2014a; Tao et al., 2012; Voigt et al., 2017; Wendisch et al., 2016). A particularly interesting region is the Amazon basin, which presents contrasting environments of aerosol particle concentration between dry and wet seasons as well as steep aerosol concentration gradients within regions with near-constant thermodynamic conditions (Andreae et al., 2004; Artaxo et al., 2013). The background number concentrations of aerosol particles and CCN over the pristine parts of the Amazon region are about a factor of 10 times lower than those of polluted continental regions, including polluted conditions over the Amazon (Martin et al., 2016). During the dry-to-wet transition season in the Amazon region, total aerosol number concentrations reach values up to 10,000 cm^{-3}, mostly due to forest fires (Andreae, 2009; Andreae et al., 2012; Artaxo et al., 2002). On the other hand, in the rainy season aerosol number concentrations are about 500-1000 cm^{-3} with CCN concentrations on the order of 200-300 cm^{-3} for 1 % supersaturation, mainly consisting of forest biogenic aerosol particles (Artaxo, 2002; Martin et al., 2016; Pöhlker et al., 2016; Pöschl et al., 2010). Additionally, Manaus city, which is located at the central Amazon basin, releases significant concentrations of urban pollution aerosol particles (e.g., due to traffic, combustion-derived particles, or different types of industrial activities). This increases CCN concentrations by up to one order of magnitude (for 0.6% supersaturation) from the wet (Green Ocean) to the dry season (Kuhn et al., 2010).

Rosenfeld et al. (2012b) showed that by estimating the adiabatic number of droplets nucleated at cloud base (N_a), the height above cloud base at which the first raindrops evolve can be parameterized. This approach is based on the assumption that the entrainment and mixing of air into convective clouds is almost completely inhomogeneous (Beals et al., 2015; Burnet and Brenguier, 2007; Freud et al., 2011; Paluch, 1979). This implies that the vertical profile of the actual cloud droplet effective radius behaves nearly as in an idealized adiabatic cloud. This connects uniquely the adiabatic drop number concentration, which is approximated by N_a at cloud base, with the adiabatic droplet effective radius (r_{ea}), based on an adiabatic parcel model for which droplet growth is dominated by condensation (Freud and Rosenfeld, 2012; Pinsky and Khain, 2002). This parameterization can be applied to estimate the height above cloud base at which raindrops start to form, when r_{ea} reaches 13 µm (D_{13}) [Freud and Rosenfeld, 2012; Konwar et al., 2012; Rosenfeld et al., 2012b; Prabha et al., 2011; VanZanten et al., 2005]. However, uncertainties associated to the calculated N_a decrease the agreement between r_{ea} and r_e. Most of these uncertainties arise when secondary activation of droplets happens above cloud base because the adiabatic model does not predict that N_d increases with height, but decrease due to evaporation and inhomogeneous cloud mixing (Pinsky and Khain, 2012).

Braga et al. (2016) applied the methodology described by Freud and Rosenfeld (2011) to calculate N_a at the base of growing convective cumulus clouds for the Amazon region during the ACRIDICON-CHUVA (Aerosol, Cloud, Precipitation, and Radiation Interactions and Dynamics of Convective Cloud Systems)-CHUVA (Cloud processes of tHe main precipitation systems in Brazil: A contribUtion to cloud resolVing modeling and to the GPM [Global Precipitation Measurements]) campaign (Wendisch et al., 2016). The N_a is calculated from $N_a = CWC_a / M_{va}$, where CWC_a is the adiabatic cloud water content (CWC_a) as calculated from cloud base pressure and temperature, and M_{va} is the adiabatic mean volume droplet mass, as approximated from the actually measured mean volume droplet mass (M_v) by the cloud probe DSDs obtained during the cloud profiling measurements. Measurements of M_v with height are considered only for cloud passes where CWC is greater than 25 % of the adiabatic CWC and r_e is lower than 11 µm (i.e. for cloud droplets which have grown mostly via condensation). The calculated N_a based on the measured vertical profile of r_e agreed well (within 20-30 %) with the actual measurements of cloud droplet number concentrations at cloud base. This approach provides the opportunity to test the agreement between estimated r_{ea} and the height above cloud base of warm rain initiation (D_r) within clouds for the Amazon region. In addition, measurements of the height above cloud base of ice initiation (D_i) in convective clouds are also available from flights that include cloud penetrations at ambient temperatures as low as -60 ºC with the High Altitude and Long Range Research Aircraft (HALO) aircraft (Wendisch et al., 2016).

This study analyzes the vertical development of cloud and precipitation particles (water drops and ice crystals) in growing convective cumulus over the Amazon, based on measurements of cloud microphysical properties from instruments mounted on HALO during ACRIDICON-CHUVA (Wendisch et al., 2016). The vertical profile of r_{ea} is used to estimate the depth above cloud base at which warm rain initiation occurs. The dominance of inhomogeneous mixing causes the r_e profile to behave almost as in adiabatic clouds, constrained by N_d at cloud base (Burnet and Brenguier, 2007; Freud et al., 2011). This means that the height above cloud base for reaching r_e of 13-14 μm, which is required for rain initiation, is also determined by cloud base N_d (Freud and Rosenfeld, 2012). Rain initiation depends strongly on r_e because the rain production rate by collision and coalescence is proportional to $\sim r_e^5$ (Freud and Rosenfeld, 2012). Here we test and quantify these relationships for the measurements conducted with HALO during ACRIDICON-CHUVA.

The HALO flights during the ACRIDICON-CHUVA campaign were performed over the Amazon region under various conditions of aerosol concentrations and land cover (Wendisch et al., 2016). Figure 1a shows the flight tracks during which cloud profile sampling in growing convective cumulus was performed. Figure 1b shows a schematic sketch of the flight pattern while sampling cloud clusters (the locations in three dimensions of each flight are available at Figure 1 on supplementary material). The aircraft obtained a composite vertical profile by penetrating young and rising convective elements, typically some 100-300 m below their tops.

The cloud droplet size distributions (DSDs) between 3-50 μm diameter were measured at a temporal resolution of 1 second by the CAS-DPOL and CCP-CDP probes (Baumgardner et al., 2001; Lance et al., 2010; Brenguier et al., 2013). Each DSD spectrum represents 1 s of flight path (covering ~150 m of horizontal distance for a typical aircraft speed). The value of r_e was calculated for each 1-s DSD. The two probes (CAS-DPOL and CCP-CDP) were mounted on opposite wings of HALO (horizontal distance of ~15 m). Similar values of N_d and derived r_e were measured by CAS-DPOL and CCP-CDP (they agree within 30 %), even though they were mounted on different wings. A previous study (Braga et al, 2016) showed that both probes were in agreement within the measurement uncertainties with respect to the measured cloud droplet number concentrations at cloud base and in accordance with the expected values for different conditions of CCN concentration and updraft wind speed below cloud base. In addition, the CWC calculated from the measured DSDs shows similar values to those measured with a hot wire device for different heights above cloud base [the probes' measurements agree within their uncertainty range (16% for probe DSDs and 30% for hot-wire device)] (Braga et al., 2016).

The determination of the height of rain initiation is based on the drizzle water content (DWC) calculation from the CCP-CIP probe (Brenguier et al., 2013). The DWC is defined as the mass of the drops integrated over the diameter range of 75–250 μm (Freud and Rosenfeld, 2012). This size range is selected because it includes only drops with terminal fall speed of 1 m s^{-1} or less, which maximizes the chance that the drizzle was formed in situ and did not fall a large distance from above. Rainwater content (RWC) is defined as the CCP-CIP integrated liquid water mass of droplets with diameters between 250 and 960 μm. The CCP-CIP images were used to distinguish raindrops and ice particles during cloud passes. The hydrometeor type is identified visually by their shapes. The phase of the smaller CCP-CIP particles cannot be distinguished. Therefore, the precipitation is considered as mixed phase when ice particles are identified, and the combined DWC and RWC are redefined as mixed phase water content (MPWC). Table 2 summarizes the calculated cloud microphysical properties with respect to the instrumentation used and its size ranges.

2. Instrumentation

2.1 Cloud particle measurements

The instrumentation used to measure cloud particles and rain or ice formation consists of three cloud probes: CAS-DPOL, CCP-CDP and CCP-CIP (Brenguier et al., 2013). In this study, cloud particle counts are accumulated for bin diameters larger than 3 µm from the CCP-CDP and CAS-DPOL; the lower size bins from these probes overlap with haze particles. Nucleated cloud drops in convective clouds grow quickly beyond 3 µm. Details about the cloud probe measurements characteristics are described in the following sub-sections and in Braga et al. (2016).

2.2.1 CCP-CDP and CCP-CIP measurements

The Cloud Combination Probe (CCP) combines two detectors, the Cloud Droplet Probe (CDP) and the greyscale Cloud Imaging Probe (CIPgs). The CDP detects forward scattered laser light of cloud particles when penetrating the CDP detection area (Lance et al., 2010). The CIP records 2-D shadow cast images of cloud elements. In this study, we deduced the existence of ice from the occurrence of visually non-spherical shapes of the shadows. The particle detection size range is 2 µm to 960 µm when measuring with the CCP at 1 Hz frequency (Wendisch et al., 2016). The combination of CCP-CDP and CCP-CIP information provides the ability to measure cloud droplets and raindrops within clouds for nearly the same air sample volume. The maximum number of particles measured by CCP-CDP and CCP-CIP are about 2,000 and 500 cm^{-3} for 1 Hz cloud pass, respectively. For the data processing of the CIP measurements, ice is assumed as the predominant particle phase in the mixed-state cloud conditions throughout the ACRIDICON-CHUVA campaign. The assumption of ice density instead of water density implies a slight overestimation (~10 %) of the calculated rain water content for particles greater than 75 µm.

2.2.2 CAS-DPOL measurements

The CAS-DPOL measures particle size distributions between 0.5 and 50 µm at 1Hz time resolution (Baumgardner et al., 2011; Voigt et al., 2010; Voigt et al., 2011). Number concentrations are derived using the probe air speed measured at the instrument. Particle inter-arrival time analysis did not show influences of coincidence (Lance, 2012). The data analysis and uncertainties are described in detail in Braga et al. (2016).

Braga et al. (2016) have shown sufficient agreement between both CAS-DPOL and CCP-CDP measurements of cloud droplet number concentration to distinguish convective clouds that develop above clean vs. polluted regions during the ACRIDICON-CHUVA campaign. In addition, the CWC estimated by integration of the DSDs measured with both probes showed good agreement with hot wire CWC measurements (Braga et al., 2016).

2.3 Meteorological data

The HALO aircraft was equipped with a meteorological sensor system (BAsic HALO Measurement And Sensor System - BAHAMAS) located at the nose of the aircraft (Wendisch et al., 2016). The uncertainties for measurements of temperature, relative humidity and vertical wind speed are 0.5 K, 5 % and 0.3 m s^{-1}, respectively (Mallaun et al., 2015).

2.4 Aerosol measurements

Aerosol particle measurements were performed using the Passive Cavity Aerosol Spectrometer Probe 100X (PCASP-100X), which is an airborne optical spectrometer that measures aerosol particles in the 0.1 µm to 3 µm diameter range (Liu et al., 1992). The maximum number of particles measured by PCASP is about 3,000 cm^{-3} for 1 Hz cloud pass. During ACRIDICON-CHUVA campaign PCASP was not operated with a heated inlet, thus, the measured aerosol particles below cloud base (about 200 m) can be larger than the original dry size due to swelling.

3. Methods

The analyses are performed along the following general steps:

a) The relationship between r_e and the probability of drizzle is defined. The value of r_e is calculated from the size distributions measured by the CAS-DPOL and the CCP-CDP (two different values). DWC, RWC, and MPWC are obtained from the CCP-CIP data.
b) The N_a at cloud base is estimated through the vertical profile of r_e.
c) The height of rain initiation based on the modeled adiabatic growth of r_e with height is estimated for different aerosol condition as a function of estimated N_a. The value of D_{13} is estimated as the cloud depth for which the adiabatic r_e reaches 13 µm.
d) The extent of agreement between the directly measured D_r within convective clouds and the estimated D_{13} based on the assumption of adiabatic r_e growth and on the measured r_e is discussed.

3.1. Estimation of r_e, rain and ice initiation

Rain is initiated during the warm phase of growing convective cumulus by intensification of the collision and coalescence (coagulation) processes with height. The efficiency of the process of droplet coalescence is determined by the collection kernel (K) of the droplets and their concentrations (Pruppacher et al., 1998). Freud and Rosenfeld (2012) have shown through model simulations and aircraft measurements that $K \propto r_v^{4.8}$, where r_v is the mean volume radius obtained from the cloud probe DSDs in the absence of ice. r_v is defined as follows:

$$r_v = \left(\frac{3\,CWC}{4\,\pi\,\rho\,N_d}\right)^{\frac{1}{3}} \qquad (1)$$

where ρ is the water density (1 g cm^{-3}), CWC is in g m^{-3}, and N_d is in cm^{-3}. The values are obtained from the 1-Hz data of droplet size distributions from the cloud probes. The calculation of CWC is performed separately with CAS-DPOL and CCP-CDP probe droplet concentrations as follows:

$$CWC = \frac{4\pi}{3}\rho \int N(r) r^3 \mathrm{d}r \qquad (2)$$

where N is the droplet concentration and r the droplet radius. The calculations of DWC, RWC, and MPWC are done in similar fashion to CWC but with different cloud probes and particle size ranges (see Table 2).
The definition of r_e is:

$$r_e = \frac{\int N(r) r^3 dr}{\int N(r) r^2 dr} \qquad (3)$$

Freud and Rosenfeld (2012) showed that $r_v \approx 1.08 \cdot r_e$, depending on the droplet size distribution. Using this relationship, they derived r_e from r_v and showed that warm rain initiates within clouds when r_e is about 13-14 µm (Klein et al., 2009; Rosenfeld and Gutman, 1994; Rosenfeld and Lensky, 1998; Rosenfeld et al., 2012a, 2014b).

Only measurements with CWC larger than 25% of the adiabatic water content are considered in order to exclude convectively diluted or dissipating clouds. It is assumed that rain (or ice) formation starts when calculated DWC exceeds 0.01 g m^{-3} (Freud and Rosenfeld, 2012). For rain initiation in liquid phase the DWC threshold is ~10% greater due to the overestimation of DWC during CIP measurements in warm clouds (as stated at Section 2.2.1). The small terminal fall speed of the drizzle drops (≤ 1 m s^{-1}) allows to focus on in-situ rain (or ice) initiation while minimizing the amount of DSDs affected by rain drops fallen from above into the region of measurements. In addition, cloud passes with rain were eliminated when cloud tops were visibly much higher than the penetration level (> ~1000 m), based on the videos recorded by the HALO's cockpit forward-looking camera. However, cloud tops higher than few hundred meters above the penetration level occurred only rarely.

Table 3 shows the cloud depth above cloud base at which warm rain initiation occurs (D_r) (i.e., DWC > 0.01 g m^{-3}) for all flights as a function of estimated N_a. The D_r is taken as the cloud depth for ice initiation (D_i) if ice particles are evident in the CCP-CIP images.

3.2. Estimating N_a and adiabatic r_e

The N_a for the convective clusters is estimated based on the slope between the calculated CWC and the mean volume droplet (M_v) for 1-s DSD measurements of CAS-DPOL and CCP-CDP for non-precipitating cloud passes (Braga et al., 2016). Braga et al. (2016) have shown that this estimated N_a was in a reasonably good agreement with the directly measured cloud base droplet number concentration, N_d, as obtained from the CCP-CDP and CAS-DPOL during ACRIDICON-CHUVA. Once N_a is estimated, the adiabatic r_e (r_{ea}) can be calculated based on a simple adiabatic parcel model where droplet growth is dominated by condensation (Pinsky and Khain, 2002).

The N_a calculated for cloud base was used to classify clouds as having developed in clean, polluted, or very polluted regions. A clean cloud case was defined as N_a < 500 cm^{-3}, polluted for 500 cm^{-3} < N_a < 900 cm^{-3}, and very polluted for N_a > 900 cm^{-3}. During ACRIDICON-CHUVA, a flight in clean clouds (AC19) was performed over the Atlantic Ocean. Clouds observed during flights over the northern Amazon were classified as polluted, mainly due to diluted smoke from biomass burning advected by long-range transport. This region represents the Amazon background condition for aerosol concentration during the dry season. Very polluted conditions were met over the Central Amazon, which was affected strongly by biomass burning over the Amazonian deforestation arc (southern Amazon).

4. Results

4.1 Threshold of r_e for warm rain initiation

The values of r_e derived from integrating the cloud probe DSDs were used to identify rain initiation. Some caution is required to eliminate possible bias resulting from peculiar shapes of the drop size spectrum. An r_e value of 13-14 µm represents the rain initiation threshold for growing convective cumulus observed at different locations in the world, as long as there is no significant influence from giant CCN (GCCN; dry soluble diameter > 1 µm) (Freud and Rosenfeld, 2012).The presence of GCCN during cloud droplet formation at cloud base can lead to a faster formation of raindrops due to both, the rain embryo effect and the competition effect that reduces cloud base maximum supersaturation and consequently reduces N_d (Rosenfeld, 2000; Segal et al., 2007). Such cases are very common over the ocean due to sea spray aerosols; there, the values of r_e at which raindrops start to form are commonly smaller than the usual threshold of

13-14 μm (Freud and Rosenfeld, 2012). In our study the DSDs from flight AC19 performed over the Atlantic Ocean did not show a large drop tail near cloud base (see Figure 2 in the supplementary material). The cumulative sample volume from CCP-CDP probe at cloud base was about 5.8 L^{-1} for 176 s of measurements. The figure shows the scarcity of large cloud droplet (with diameters > 20 μm) near cloud base, where the mean concentration of such droplets is smaller than 0.1 drop cm^{-3}. Such small concentration of large droplets at cloud base is insufficient to have any significant effect on supersaturation.

Figures 2a-b show the precipitation initiation probability as a function of r_e calculated from the CCP-CDP and CAS-DPOL probes for all flights analyzed over the Amazon. The precipitation probability is calculated by integrating the measured DSDs exceeding certain DWC thresholds. These figures show that for the CCP-CDP probe rain initiation is expected to occur at r_e > 13 μm, whilst for CAS-DPOL the rain initiation threshold is r_e > 12 μm. Difference of the two instruments in the r_e range below ~7 μm and above ~11 μm have been discussed in Braga et al. (2016). For r_e < 7 μm, they are related to a higher sensitivity of the CAS-DPOL for small cloud and aerosol particles, whereas for r_e > 11 μm CAS-DPOL has lower sensitivity to large particles than CCP-CDP; however the differences are not significant within the uncertainties of the measurements. According to Figure 3, the r_e calculated with the DSD measured with the CCP-CDP is about ~7% higher than the r_e calculated from CAS-DPOL data.

Figures 4a-b show the relationship between r_e and r_v calculated for both cloud probes. The figure shows slight differences between the probes, with $r_v \sim 1.065 \cdot r_e$ for CCP-CDP and $r_v \sim 1.085 \cdot r_e$ for CAS-DPOL [which is closer to what was found by Freud and Rosenfeld (2012), where $r_v \sim 1.08 \cdot r_e$]. The agreement between these probes and theoretical models, shown by Braga et al. (2016), supports their use for closure analysis between r_{ea} and r_e calculated from measured DSDs as a function of cloud depth above cloud base (D_c). Because the CCP-CDP was mounted very close to the CCP-CIP, results from this probe are shown in subsequent sections; similar results were found from data collected with the CAS-DPOL probe.

4.2 Comparing estimated r_{ea} *with measured* r_e

The comparison between the values of r_{ea} (calculated from the estimated N_a at cloud base described in Section 3.2) with the measured r_e is the basis for analyzing the evolution of cloud particle size until rain or glaciation initiation occurs within the cloud. Rosenfeld et al. (2012b) showed that a tight relationship between the N_a calculated for cloud base and the evolution of r_{ea} with height (r_{ea}-D_c) provides a useful proxy of the depth in convective clouds at which raindrops start to form.

4.2.1 Case study: Flight AC07 over the Amazon deforestation arc

Flight AC07 was performed over the deforestation arc (see Figure 1a). Figure 5 shows the number of droplets measured at different heights in the convective clouds. Droplet concentrations reaching ~2000 cm^{-3} were measured at cloud base, which is characteristic for very polluted clouds. The cloud base was located at about 1900 m above sea level, with ambient air temperature at about 16ºC. Figure 6a shows the mean DSD for a cloud penetration at cloud base. It emphasizes the higher number concentration of small droplets (< 10 μm) that are observed in convective clouds forming in polluted environments. Figure 6b shows the evolution of r_e measurements and estimated r_{ea} as a function of temperature. The figure also shows that the values of r_e do not exceed the 13 μm threshold at warm temperatures. These results suggest that cloud droplets formed at cloud base grow mainly via condensation and no raindrops were formed during the warm phase of convective cloud development. However, to rule out coalescence processes as a possible reason for droplet growth, further analysis using CCP-CIP images was done.

Figures 7a-c show the evolution of DSD and CWC (mean values) as a function of height above cloud base and the cloud particle images from the CCP-CIP. Figure 7a plots the data for a cloud pass at warm temperatures and Figures 7b-c result from measurements during cloud passes at cold temperatures. The DSDs show that most droplets have a diameter smaller than 20 µm, and only very few large droplets are observed for warm temperatures. The CCP-CIP detected only cloud droplets and no raindrops, as evident by both RWC and DWC < 0.01 gm^{-3}. At cold temperatures, the CCP-CIP images show the irregular shapes of large ice particles. No spherical raindrop shapes were found in these data for any of the cloud passes, including those collected at warm temperatures. The DWC and RWC calculated from the mean DSDs show values greater than zero only when ice particles were observed on the CCP-CIP images. Also, for a cumulative sample volume of 1.24 m^{-3} from 89 s of CCP-CIP measurements, no raindrop were observed between the heights above cloud base of 2,900 m (0ºC) and 7,100 m (-26.25 ºC). This means that the raindrop concentration, if any, was smaller than 1 drop m^{-3}. This is a negligible rain rate, and supports the notion of practical shut of coalescence. Furthermore, the CCP-CIP did not detect any raindrops at lower levels (warm temperatures) for a cumulative sample volume of 5.9 m^{-3} from 426 s of measurements. These results indicate a strong inhibition of raindrop formation within growing convective cumulus for this flight over the deforestation arc of the Amazon. Even though some of the indicated effective radii values are larger than 13 µm for colder temperatures, these values do not indicate rain formation when only ice particles are observed. This does not exclude the possibility that small raindrops froze soon after their formation in such low temperatures.

The mean DSD and CIP images shown in Figure 7c result from a passage through a convective cloud with lightning activity. Figure 8 shows a photo of the cloud taken from the HALO cockpit just before the cloud penetration. The CCP-CIP has imaged graupel in this case. The presence of these type of ice particles within convective clouds is very common in thunderstorms, and previous studies highlight the large frequency of lightning occurrence during the dry-to-wet season over the deforestation arc region of the Amazon (Albrecht et al., 2011; Williams et al., 2002). These results also highlight the role of aerosols from biomass burning on warm rain inhibition and on the aerosol invigoration effect due to the generation of large ice particles and lightning (Rosenfeld et al., 2008).

Regarding the values of r_e as a function of D_c, Figure 9a shows the estimated r_{ea} (calculated from the adiabatic CWC shown at Figure 9b) and measured r_e. The figure shows that the estimated values for r_{ea} are close to the r_e measurements for convective cloud passes at different D_c. Even though no raindrops were observed in the convective cloud, the figure shows similar values of r_{ea} and measured r_e (with r_{ea} slightly larger) as a function of D_c.

4.2.2 Analysis of r_e and D_c in clean and polluted regions

- Clean region

Figure 10a shows the measured N_d of a convective cluster over the Atlantic Ocean off the Brazilian coast (flight AC19). This region was classified as clean because N_a is about 300 cm^{-3} (see Table 3). The cloud base was located at 600 m above sea level at a temperature of 23 ºC. Given the clean conditions over the ocean, the high relative humidity at surface level and the low concentration of CCN lead to the formation of large droplets already close to cloud base. Figure 10b shows the estimated r_{ea} and the measured r_e as a function of D_c. Several cloud passes showed large droplets with r_e ~ 13 µm at only 1660 m above cloud base. Figures 11a-b show the DSDs and CCP-CIP images for the cloud passes at the height where rain starts to form and at the greatest height measured above cloud base, respectively. Figure 11a shows that rain is initiated (DWC > 0.01 g m^{-3}) already when the droplets become larger than about r_e > 12 µm. This is probably due to the presence of GCCN over this maritime region.

Figure 12 shows the mean aerosol particle size distribution (PSD), as measured by the PCASP, just below cloud base for clean, polluted, and very polluted regions. The mean total number concentration of aerosol particles with sizes larger than 0.1 µm is about 1000 cm^{-3} over the Atlantic Ocean, whilst for polluted (very polluted) case this value is about three (ten) times larger. In addition, the mean total number concentration of particles measured by the CCP-CDP show concentration ten times greater for particles larger than 10 µm over the ocean in comparison with inland Amazon region. This figure indicates the presence of large aerosols particles with sizes greater than 1 µm (possibly GCCN) over the ocean. When it nucleates droplets, this type of aerosol accelerates the growth of droplets during the warm phase leading to a faster formation of raindrops than predicted by the adiabatic parcel model. About 3500 m above cloud base, large raindrops are observed in the CCP-CIP images (see Figure 11b). The low CWC indicates that most of it was already converted into raindrops. These results highlight that under clean conditions, raindrops were formed mainly by warm phase processes of cloud development. Even if the convective clouds reach colder temperatures, the low remaining amount of cloud water reduced a key ingredient for cloud electrification.

Before raindrops start to form (Dc ~1,660 m) updrafts were observed with most values < 4 m s^{-1}, and when rain starts downdrafts starts to be evident (see Figure 3g at supplementary material). The values of vertical velocities measured at flight AC19 (clean region) were smaller than measured for flight AC07 (very polluted region). However, for both cases updrafts are more evident during droplets growth via condensation and downdrafts are stronger when precipitation particles are observed in the cloud. Strong updrafts (~10 m s^{-1}) are observed in polluted cases after ice starts to form, probably due to the latent heat release during freezing processes. An alternative explanation of updraft enhancement due to environmental conditions in these cases cannot be excluded.

-Polluted regions

The flights AC09 and AC18 were classified as polluted (see Table 3). These flights were performed over the northern Amazon region (see Figure 1a). Figure 13a shows the measured N_d from flight AC09. The cloud base was located about 1200 m above sea level at a temperature of 19.5 ºC. Figure 13b shows the estimated r_{ea} and the measured r_e as a function of D_c. Values of r_e > 13 µm were observed for temperatures around 0 ºC, indicating the possibility of rain starting at this height. Figure 14a-b shows the DSDs and CCP-CIP images from flight AC09 at the height where rain starts to form (D_r ~3000 m) and at the greatest height with measurements above cloud base. The CIP image at Figure 14b shows the first pass in which ice hydrometeors are observed mixed with supercooled rain drops. For lower levels only raindrops were observed. For flight AC18 cloud base was located about 1700 m above sea level at a temperature of 17 ºC, and rain started to form in convective clouds when D_r ~3800 m. Figure 5a at the supplementary material shows that first rain drops in AC18 are observed at the -5.7 ºC isotherm, and that they still remain liquid, or at least spherical, at the -11.4 ºC isotherm (see Figure 5b at the supplementary material). Larger raindrops and a high amount of DWC were observed on AC09 for warmer temperatures than on flight AC18 (not shown). These results show that differences in cloud particle formation are associated with the D_c at which convective clouds start to form raindrops or ice, defined earlier as D_r and D_i. Flight AC18 has a droplet concentration, N_d, of up to 100 cm^{-3} greater than the measurements during AC09. With higher N_d at cloud base, droplet growth via condensation in convective clouds is a less pronounced function of height due to the water vapor competition between droplets. Under these conditions, the collision and coalescence process and freezing of droplets are initiated at higher D_c (Freud and Rosenfeld, 2012; Rosenfeld et al., 2008). For this the reason, the formation of raindrops and ice particles on flight AC09 starts at lower D_c than on flight AC18 (assuming non-significant secondary drop activation above cloud base).

-Very polluted regions

Five flights were classified as very polluted (see Table 3): AC07, AC08, AC12, AC13, and AC20. The microphysical analysis of the measurements collected in growing convective cumulus during flight AC07 was already presented in Section 4.2.1. Figure 15a show the measured N_d from flight AC13, which was made in the same region as flight AC07. The figure shows that the values of N_d near cloud base on flight AC13 reach 2000 cm^{-3}, similar to AC07. However, the rate of decrease of N_d with height above cloud base is much smaller in AC13 compared to AC07. During flight AC13 the measurements of large updrafts (which increase supersaturation and induce new droplets activation) and large aerosol concentration above cloud base suggest the occurrence of secondary activation leading to the observed relative increase of N_d with height. This is supported by the fact that the observed r_e are smaller than the calculated r_{ea}, as shown in Figure 15b. Only values below 13 µm are observed (maximum of 12 µm), indicating the suppression of raindrop formation. Indeed, no raindrops were observed in the CCP-CIP images from growing convective cumulus passes on this flight, and only cloud droplets and ice particles were detected. Figure 16 shows the DSD and CCP-CIP images at the start of glaciation (D_i ~4800 m). These results highlight the role of aerosols in inhibition of raindrop formation due to inducing a larger N_d and respective lower r_e, which leads to suppression of collision and coalescence processes in very polluted regions.

The measured N_d during flights AC08, AC12, and AC20 was greater above cloud base than at cloud base on several cloud passes (especially in flights AC08 and AC20; see Figures 6 and 7 in the supplementary material for these flights). In these flights the estimated r_{ea} values were larger than the measured r_e as a function of D_c and strong updrafts (up to 15 m s^{-1}) were observed above cloud base (see Figures 3b,d and h in the supplementary material). The acceleration of updrafts above the height of cloud base increase supersaturation and thus can induce secondary drop activation. For flights which we observed the increase of N_d with height, high aerosol concentration was observed indicating secondary nucleation of droplets above cloud base. During these flights, cloud profiling was performed up to D_c ~3500 m, and the values of measured r_e were smaller than 13 µm, indicating the suppression of raindrop formation. The analysis of the data from the cloud probe DSDs and CCP-CIP images indicates that indeed no raindrops were present on these flights (not shown). The measurements from AC07 and AC13 over very polluted regions in the Amazon suggest that no raindrops are formed in growing convective clouds under these conditions. Instead, large precipitation particles are formed at cold temperatures in the form of ice. The D_c at which these ice particles are formed depends on the size of the cloud droplets (r_e) at colder temperatures (larger droplets freeze earlier or at lower D_c) [Pruppacher et al., 1998]. This was previously documented by satellite retrievals (Rosenfeld et al., 2011), where glaciation temperatures of convective clouds were strongly dependent on r_e at the -5 °C isotherm, where smaller r_e were correlated with lower glaciation temperatures.

4.2.3 Discussion

The results from cloud probe measurements under clean, polluted, and very polluted conditions highlight the role of aerosol particles in rain and ice formation for growing convective cumulus. Figure 17 summarizes the estimated depths above cloud base at which initiation of rain and ice formation is observed (D_r and D_i), as well as the estimated D_c for rain initiation as indicated from r_{ea} by D_{13}. This figure shows a close relationship between N_a and D_r of $D_r = (5\pm0.7)N_a$, demonstrating the capability to predict the minimum height at which raindrops are expected to form based on cloud base drop concentrations. For flights in which rain was observed (AC19, AC18, and AC09), D_r occurs at heights slightly greater than D_{13}. For cases where neither rain nor ice were observed (AC08, AC12, and AC20), the estimated D_{13} was not reached during the HALO cloud profiling flights. In addition, D_{13} and D_i show similar values for flight AC07, whereas for flight AC13 the values are less comparable (probably due to an overestimation of N_a, and thus D_{13}, caused by secondary activation above cloud base).

The linear relationship between N_a and D_{13} indicates a regression slope of about 5 m $(cm^{-3})^{-1}$ between D_{13} and the calculated N_a for the Amazon during the dry-to-wet season. This value is slightly larger than the values observed by Freud and Rosenfeld (2012) for other locations around the globe (e.g., India and Israel).

For the flight in cleanest conditions (AC19), the presence of larger aerosol particles (possibly GCCN from sea spray) below cloud base leads to a faster growth of cloud droplets via condensation with height, and consequently r_e is smaller than 13 µm (see Figure 11a) for warm rain initiation. A similar decrease of r_e for rain initiation over ocean was observed by Konwar et al. (2012). While D_r is explained by N_d and well correlated with it, there is no correlation between N_d and D_i.

Figure 18 summarizes the findings for all the vertical profiling flights. It illustrates the vertical development of precipitation water content by symbols representing the amount of DWC and MPWC as a function of D_c and CDP-measured r_e. Also shown are the lines of r_{ea} as a function of D_c. The figure shows that raindrops began to form at r_e of 13 µm for AC09 and AC18. The r_e for rain initiation is slightly smaller (12 µm) on AC19; probably due to the sea spray giant CCN, which accelerate the coalescence for a given r_e. Mixed phase precipitation was initiated on flights AC07 and AC13, well below the height of D_{13} at an r_e of 12 and 10 µm, respectively. Ice starts to form at lower temperatures when the cloud droplets are smaller, as manifested by D_i of -9 and -14 °C for flights AC07 and AC13, respectively. The remaining flights did not reach the height for rain initiation (AC08, AC12, and AC20).

It is evident that raindrops form faster via collision and coalescence process in a cleaner atmosphere. For the polluted cases, raindrops form at colder temperatures (~0 ºC and colder) via collision and coalescence than for clean conditions. Rain can initiate at supercooled temperatures, e,g., -5 °C on AC18. The raindrops were documented to start freezing at -9 °C in AC09. In very polluted conditions, only cloud droplets, but no raindrops were observed at D_c < 4000 m. In these cases, precipitation was initiated as ice particles at D_c > 4000 m. These flights with completely suppressed warm rain were performed over the smoky deforestation arc. Measurements of large updrafts which increase supersaturation within cloud and the higher N_d above cloud base indicate new activation of cloud droplets for flight AC13 (not observed at AC07) in the course of the development of convective cumulus. This secondary activation leads to smaller r_e. For flights where secondary activation was significant, the differences between the estimated r_{ea} and the r_e measurements at same height are larger, because the adiabatic estimation does not consider the secondary activation of droplets above cloud base and thus overestimates the observed size.

5. Conclusions

This study focused on the effects of aerosol particle number concentration on the initiation of rain drops and ice hydrometeors in growing convective cumulus over the Amazon. Data from aerosol and cloud probes on board of the HALO aircraft were used in the analysis. The values of the estimated N_a at cloud base were applied to classify the atmospheric conditions where convective clouds developed as a function of aerosol particle number concentration (i.e., clean, polluted, and very polluted regions). From the estimated N_a, the evolution of r_{ea}, the theoretical r_e assuming adiabatic growth of droplets, with cloud depth above cloud base (D_c) were compared with the observed r_e at the various heights. A DWC value of 0.01 g m^{-3} was used as a threshold for rain initiation or glaciation within clouds. Images from the CCP-CIP probe were used to detect the presence of raindrops and/or ice hydrometeors. The results support the use of r_e ~ 13-14 µm as a threshold for rain initiation in convective clouds. The evolution of the directly observed r_e follows that of the calculated r_{ea} with slight differences as a function of aerosol particle size distributions. Rain initiation occurred higher in more polluted clouds, as manifested by higher D_c. Rain was initiated at supercooled levels in moderately polluted clouds. In very polluted conditions, warm rain was suppressed completely. This was exacerbated by the occurrence of secondary activation above cloud base, which further reduced r_e compared to r_{ea}. The initiation of ice hydrometeors is also delayed to greater D_c in more polluted clouds, because smaller drops freeze at colder temperatures. Ice was initiated mostly by freezing raindrops in cases when warm rain formation was not completely suppressed. Both the D_{13} and D_r increased linearly with N_a, in agreement with the theoretical considerations of Freud and Rosenfeld (2012). Despite the suspected occasional secondary drop activation, r_e was sufficiently close to r_{ea} to allow a linear relationship in the form of $D_r = (5±0.7)N_a$. The observations suggest also that, in the absence of new droplet activation above cloud base, D_{13} is very similar to D_i under very polluted conditions, where raindrops are not formed at warmer temperatures.

These results show that even moderate amounts of smoke, which fill most of the Amazon basin during the drier season, are sufficient to suppress warm rain and elevate its initiation to above the 0 ºC isotherm level. This results in a suppression of rain from small clouds and an invigoration in the deep clouds, as hypothesized by Rosenfeld et al. (2008). While the net effect on rainfall amount is unknown, the redistribution of rain intensities and the resulting vertical latent heating profiles are likely to affect the regional hydrological cycle in ways that need to be studied further.

Acknowledgements

The first two authors of this study were supported by project BACCHUS European Commission FP7-603445. The generous support of the ACRIDICON-CHUVA campaign by the Max Planck Society, the German Aerospace Center (DLR), FAPESP (São Paulo Research Foundation), and the German Science Foundation (Deutsche Forschungsgemeinschaft, DFG) within the DFG Priority Program (SPP 1294) "Atmospheric and Earth System Research with the Research Aircraft HALO (High Altitude and Long Range Research Aircraft)" is greatly appreciated. This study was also supported by EU Project HAIC under FP7-AAT-2012-3.5.1-1. C. Mahnke and R. Weigel received funding by the German Federal Ministry of Education and Research (BMBF, Bundesministerium für Bildung und Forschung) within the joint ROMIC-project SPITFIRE (01LG1205A). In addition, the German Science Foundation within DFG SPP 1294 HALO by contract no VO1504/4-1 and contract no JU 3059/1-1 contribute to support this study. The first author also acknowledges the financial support from the Brazilian funding agencies CAPES and CNPq during his Ph.D. studies.

References

Albrecht, R. I., Morales, C. A. and Silva Dias, M. A. F.: Electrification of precipitating systems over the Amazon: Physical processes of thunderstorm development, J. Geophys. Res., 116(D8), D08209, doi:10.1029/2010JD014756, 2011.

Andreae, M. O.: Correlation between cloud condensation nuclei concentration and aerosol optical thickness in remote and polluted regions, Atmos. Chem. Phys., 9(2), 543–556, doi:10.5194/acp-9-543-2009, 2009.

Andreae, M. O., Rosenfeld, D., Artaxo, P., Costa, A. A., Frank, G. P., Longo, K. M. and Silva-Dias, M. A. F.: Smoking rain clouds over the Amazon., Science, 303(5662), 1337–42, doi:10.1126/science.1092779, 2004.

Andreae, M. O., Artaxo, P., Beck, V., Bela, M., Freitas, S., Gerbig, C., Longo, K., Munger, J. W., Wiedemann, K. T. and

Wofsy, S. C.: Carbon monoxide and related trace gases and aerosols over the Amazon Basin during the wet and dry seasons, Atmos. Chem. Phys., 12(13), 6041–6065, doi:10.5194/acp-12-6041-2012, 2012.

Artaxo, P., Martins, J. V., Yamasoe, M. A., Procópio, A. S., Pauliquevis, T. M., Andreae, M. O., Guyon, P., Gatti, L. V. and Leal, A. M. C.: Physical and chemical properties of aerosols in the wet and dry seasons in Rondônia, Amazonia, J. Geophys. Res. D Atmos., 107(20), 1–14, doi:10.1029/2001JD000666, 2002.

Artaxo, P., Rizzo, L. V, Brito, J. F., Barbosa, H. M. J., Arana, A., Sena, E. T., Cirino, G. G., Bastos, W., Martin, S. T. and Andreae, M. O.: Atmospheric aerosols in Amazonia and land use change: from natural biogenic to biomass burning conditions, Faraday Discuss., 165, 203–235, doi:10.1039/C3FD00052D, 2013.

Baumgardner, D., Brenguier, J. L., Bucholtz, A., Coe, H., DeMott, P., Garrett, T. J., Korolev, A., Krämer, M., Petzold, A., Strapp, W., Pilewskie, P., Taylor, J., Twohy, C., Wendisch, M., Bachalo, W., and Chuang, P. Airborne instruments to measure atmospheric aerosol particles, clouds and radiation: A cook's tour of mature and emerging technology. *Atmospheric Research*, *102*(1), 10-29, 2011.

Beals, M. J., Fugal, J. P., Shaw, R. A., Lu, J., Spuler, S. M. and Stith, J. L.: Holographic measurements of inhomogeneous cloud mixing at the centimeter scale, , 350(6256), 87–90, doi:10.1126/science.aab0751, 2015.

Braga, R. C., Rosenfeld, D., Weigel, R., Jurkat, T., Andreae, M. O., Wendisch, M., Pöhlker, M. L., Klimach, T., Pöschl, U., Pöhlker, C., Voigt, C., Mahnke, C., Borrmann, S., Albrecht, R. I., Molleker, S., Vila, D. A., Machado, L. A. T., and Artaxo, P.: Comparing calculated microphysical properties of tropical convective clouds at cloud base with measurements during the ACRIDICON-CHUVA campaign, Atmos. Chem. Phys. Discuss., doi:10.5194/acp-2016-872, in review, 2016.

Brenguier, J. L., Bachalo, W. D., Chuang, P. Y., Esposito, B. M., Fugal, J., Garrett, T., Gayet, J. F., Gerber, H., Heymsfield, A., Kokhanovsky, A., Korolev, A., Lawson, R. P., Rogers, D. C., Shaw, R. A., Strapp, W. and Wendisch, M.: In Situ Measurements of Cloud and Precipitation Particles, in Airborne Measurements for Environmental Research: Methods and Instruments, pp. 225–301., 2013.

Burnet, F. and Brenguier, J.L.: Observational Study of the Entrainment-Mixing Process in Warm Convective Clouds, J. Atmos. Sci., 64(6), 1995–2011, doi:10.1175/JAS3928.1, 2007.

Chen, R., R. Wood, Z. Li, R. Ferraro, and F. Chang: Studying the vertical variation of cloud droplet effective radius using ship and spaceborne remote sensing data, J. Geophys. Res., 113, D00A02, doi:10.1029/2007JD009596, 2008.

Fan, J., Leung, L. R., Demott, P. J., Comstock, J. M., Singh, B., Rosenfeld, D., Tomlinson, J. M., White, A., Prather, K. A., Minnis, P., Ayers, J. K. and Min, Q.: Aerosol impacts on California winter clouds and precipitation during calwater 2011: Local pollution versus long-range transported dust, Atmos. Chem. Phys., 14(1), 81–101, doi:10.5194acp-14-81-2014f, 2014.

Freud, E. and Rosenfeld, D.: Linear relation between convective cloud drop number concentration and depth for rain initiation, J. Geophys. Res. Atmos., 117(2), 1–13, doi:10.1029/2011JD016457, 2012.

Freud, E., Rosenfeld, D. and Kulkarni, J. R.: Resolving both entrainment-mixing and number of activated CCN in deep convective clouds, Atmos. Chem. Phys., 11(24), 12887–12900, doi:10.5194/acp-11-12887-2011, 2011.

Frey, W., Borrmann, S., Kunkel, D., Weigel, R., De Reus, M., Schlager, H., Roiger, A., Voigt, C., Hoor, P., Curtius, J., Krämer, M., Schiller, C., Volk, C. M., Homan, C. D., Fierli, F., Di Donfrancesco, G., Ulanovsky, A., Ravegnani, F., Sitnikov, N. M., Viciani, S., D'Amato, F., Shur, G. N., Belyaev, G. V., Law, K. S. and Cairo, F.: In situ measurements of tropical cloud properties in the West African Monsoon: Upper tropospheric ice clouds, mesoscale convective system outflow, and subvisual cirrus, Atmos. Chem. Phys., 11(12), 5569–5590, doi:10.5194/acp-11-5569-2011, 2011.

Gerber, H.: Microphysics of marine stratocumulus clouds with two drizzle modes, J. Atmos. Sci., 53(12), 1649–1662, 1996.

Khain, A., Rosenfeld, D. and Pokrovsky, A.: Aerosol impact on the dynamics and microphysics of deep convective clouds, Q. J. R. Meteorol. Soc., 131, 2639–2663 ST – Aerosol impact on the dynamics and, doi:10.1256/qj.04.62, 2005.

Khain, A., Ovtchinnikov, M., Pinsky, M., Pokrovsky, A. and Krugliak, H.: Notes on the state-of-the-art numerical modeling of cloud microphysics, Atmos. Res., 55(3-4), 159–224, doi:10.1016/S0169-8095(00)00064-8, 2000.

Klein, S. A., McCoy, R. B., Morrison, H., Ackerman, A. S., Avramov, A., Boer, G. De, Chen, M., Cole, J. N. S., Del Genio, A. D., Falk, M., Foster, M. J., Fridlind, A., Golaz, J.C., Hashino, T., Harrington, J. Y., Hoose, C., Khairoutdinov,

Konwar, M., Maheskumar, R. S., Kulkarni, J. R., Freud, E., Goswami, B. N. and Rosenfeld, D.: Aerosol control on depth of warm rain in convective clouds, J. Geophys. Res. Atmos., 117(13), 1–10, doi:10.1029/2012JD017585,2012, 2012.

Kuhn, U., Ganzeveld, L., Thielmann, A., Dindorf, T., Schebeske, G., Welling, M., Sciare, J., Roberts, G., Meixner, F. X., Kesselmeier, J., Lelieveld, J., Kolle, O., Ciccioli, P., Lloyd, J., Trentmann, J., Artaxo, P. and Andreae, M. O.: Impact of Manaus City on the Amazon Green Ocean atmosphere: ozone production, precursor sensitivity and aerosol load, Atmos. Chem. Phys., 10(19), 9251–9282, doi:10.5194/acp-10-9251-2010, 2010.

Lance, S.: Coincidence errors in a cloud droplet probe (CDP) and a cloud and aerosol spectrometer (CAS), and the improved performance of a modified CDP, J. Atmos. Ocean. Technol., 29(10), 1532–1541, doi:10.1175/JTECH-D-11-00208.1, 2012.

Lance, S., Brock, C. A., Rogers, D. and Gordon, J. A.: Water droplet calibration of the Cloud Droplet Probe (CDP) and in-flight performance in liquid, ice and mixed-phase clouds during ARCPAC, Atmos. Meas. Tech., 3(6), 1683–1706, doi:10.5194/amt-3-1683-2010, 2010.

M. F., Larson, V. E., Liu, X., Luo, Y., McFarquhar, G. M., Menon, S., Neggers, R. A. J., Park, S., Poellot, M. R., Schmidt, J. M., Sednev, I., Shipway, B. J., Shupe, M. D., Spangenberg, D. A., Sud, Y. C., Turner, D. D., Veron, D. E., Salzen, K. Von, Walker, G. K., Wang, Z., Wolf, A. B., Xie, S., Xu, K.-M., Yang, F. and Zhang, G.: Intercomparison of model simulations of mixed-phase clouds observed during the ARM Mixed-Phase Arctic Cloud Experiment. I: single-layer cloud, Q. J. R. Meteorol. Soc., 135(641), 979–1002, doi:10.1002/qj.416, 2009.

Lee, G. W., Seed, A. W. and Zawadzki, I.: Modeling the variability of drop size distributions in space and time, J. Appl. Meteorol. Climatol., 46(6), 742–756, doi:10.1175/JAM2505.1, 2007.

Li, Z., Li, C., Chen, H., Tsay, S. C., Holben, B., Huang, J., Li, B., Maring, H., Qian, Y., Shi, G., Xia, X., Yin, Y., Zheng, Y. and Zhuang, G.: East Asian Studies of Tropospheric Aerosols and their Impact on Regional Climate (EAST-AIRC): An overview, J. Geophys. Res. Atmos., 116(4), doi:10.1029/2010JD015257, 2011.

Liu, P. S. K., Leaitch, W. R., Strapp, J. W., and Wasey, M. A., Response of Particle Measuring Systems airborne ASASP and PCASP to NaCl and latex particles: Aerosol Sci. Tech., 16, 83-95, 1992.

Machado L, Silva Dias M, Morales C, Fisch G, Vila D, Albrecht R, Goodman S, Calheiros A, Biscaro T, Kummerow C, Cohen J, Fitzjarrald D, Nascimento E, Sakamoto M, Cunningham C, Chaboureau J, Petersen W, Adams D, Baldini L, Angelis C, Sapucci L, Salio P, Barbosa H, Landulfo E, Souza R, Blakeslee R, Bailey J, Freitas S, Lima W, Tokay A , The Chuva Project: How Does Convection Vary across Brazil?, Bull. Am. Meteorol. Soc., doi: 10.1175/BAMS-D-13-00084.1, 2014.

Mallaun, C., Giez, A. and Baumann, R.: Calibration of 3-D wind measurements on a single-engine research aircraft, Atmos. Meas. Tech., 8(8), 3177–3196, doi:10.5194/amt-8-3177-2015, 2015.

Martin, S. T., Artaxo, P., Machado, L. A. T., Manzi, A. O., Souza, R. A. F., Schumacher, C., Wang, J., Andreae, M. O., Barbosa, H. M. J., Fan, J., Fisch, G., Goldstein, A. H., Guenther, A., Jimenez, J. L., Pöschl, U., Silva Dias, M. A., Smith, J. N. and Wendisch, M.: Introduction: Observations and Modeling of the Green Ocean Amazon (GoAmazon2014/5), Atmos. Chem. Phys., 16(8), 4785–4797, doi:10.5194/acp-16-4785-2016, 2016.

Paluch, I. R. (1979). The entrainment mechanism in Colorado cumili. J. Atmos. Sci., 36:2467–2478

Pinsky, M. B. and Khain, A.: Effects of in-cloud nucleation and turbulence on droplet spectrum formation in cumulus clouds, Q. J. R. Meteorol. Soc., 128(580), 501–533, doi:10.1256/003590002321042072, 2002.

Pöhlker, M. L., Pöhlker, C., Klimach, T., Angelis, I. H. de, Barbosa, H. M. J., Brito, J., Samara Carbone, Cheng, Y., Chi, X., Ditas, F., Ditz, R., Gunthe, S. S., Kesselmeier, J., Könemann, T., Lavrič, J. V., Martin, S. T., Moran-Zuloaga, D., Rose, D., Saturno, J., Su, H., Thalman, R., Walter, D., Wang, J., Wolff, S., Artaxo, P., Andreae, M. O. and Pöschl, U.: Long-term observations of atmospheric aerosol , cloud condensation nuclei concentration and hygroscopicity in the Amazon rain forest – Part 1 : Size-resolved characterization and new model parameterizations for CCN prediction, Atmos. Chem. Phys., (July), doi:10.5194/acp-2016-519, 2016.

Pöschl, U., Martin, S. T., Sinha, B., Chen, Q., Gunthe, S. S., Huffman, J. A., Borrmann, S., Farmer, D. K., Garland, R.

M., Helas, G., Jimenez, J. L., King, S. M., Manzi, A., Mikhailov, E., Pauliquevis, P., Petters, M. D., Prenni, A. J., Roldin, P., Rose, D., Schneider, J., Su, H., Zorn, S. R., Artaxo, P. and Andreae, M. O.: Rainforest Aerosols as Biogenic Nuclei of Clouds and Precipitation in the Amazon, Science (80-.)., 329(2010), 1513–1516, doi:10.1126/science.1191056, 2010.

Prabha, T. V., A. Khain, R. S. Maheshkumar, G. Pandithurai, J. R. Kulkarni, M. Konwar, and B. N. Goswami: Microphysics of premonsoon and monsoon clouds as seen from i n situ measurements during the Cloud Aerosol Interaction and Precipitation Enhancement Experiment (CAIPEEX), J. Atmos. Sci., 68, 1882– 1901, 2011.

Pruppacher, H. R., Klett, J. D. and Wang, P. K.: Microphysics of Clouds and Precipitation, Aerosol Sci. Technol., 28, 381–382, doi:10.1080/02786829808965531, 1998.

Ramanathan, V., Crutzen, P. J., Lelieveld, J., Mitra, A. P., Althausen, D., Anderson, J., Andreae, M. O., Cantrell, W., Cass, G. R., Chung, C. E., Clarke, A. D., Coakley, J. A., Collins, W. D., Conant, W. C., Dulac, F., Heintzenberg, J., Heymsfield, A. J., Holben, B., Howell, S., Hudson, J., Jayaraman, A., Kiehl, J. T., Krishnamurti, T. N., Lubin, D., McFarquhar, G., Novakov, T., Ogren, J. A., Podgorny, I. A., Prather, K., Priestley, K., Prospero, J. M., Quinn, P. K., Rajeev, K., Rasch, P., Rupert, S., Sadourny, R., Satheesh, S. K., Shaw, G. E., Sheridan, P. and Valero, F. P. J.: Indian Ocean Experiment: An integrated analysis of the climate forcing and effects of the great Indo-Asian haze, J. Geophys. Res., 106(D22), 28371, doi:10.1029/2001JD900133, 2001.

Rosenfeld, D.: Suppression of Rain and Snow by Urban and Industrial Air Pollution, Science (80-.)., 287, 1793–1796, doi:10.1126/science.287.5459.1793, 2000.

Rosenfeld, D. and Gutman, G.: Retrieving microphysical properties near the tops of potential rain clouds by multispectral analysis of AVHRR data, Atmos. Res., 34(1-4), 259–283, doi:10.1016/0169-8095(94)90096-5, 1994.

Rosenfeld, D. and Lensky, I. M.: Satellite-Based Insights into Precipitation Formation Processes in Continental and Maritime Convective Clouds, Bull. Am. Meteorol. Soc., 79(11), 2457–2476, doi:10.1175/1520-0477, 1998.

Rosenfeld, D. and Woodley, W. L. W.: Deep convective clouds with sustained supercooled liquid water down to -37.5 degrees C, Nature, 405(6785), 440–2, 2000.

Rosenfeld, D., Lohmann, U., Raga, G. B., O'Dowd, C. D., Kulmala, M., Fuzzi, S., Reissell, A. and Andreae, M. O.: Flood or drought: how do aerosols affect precipitation?, Science, 321(5894), 1309–13, doi:10.1126/science.1160606, 2008.

Rosenfeld, D., Yu, X., Liu, G., Xu, X., Zhu, Y., Yue, Z., Dai, J., Dong, Z., Dong, Y. and Peng, Y.: Glaciation temperatures of convective clouds ingesting desert dust, air pollution and smoke from forest fires, Geophys. Res. Lett., 38(21), 2006–2010, doi:10.1029/2011GL049423, 2011.

Rosenfeld, D., Wang, H. and Rasch, P. J.: The roles of cloud drop effective radius and LWP in determining rain properties in marine stratocumulus, Geophys. Res. Lett., 39(13), 1–6, doi:10.1029/2012GL052028, 2012a.

Rosenfeld, D., Williams, E., Andreae, M. O., Freud, E., Pöschl, U. and Rennó, N. O.: The scientific basis for a satellite mission to retrieve CCN concentrations and their impacts on convective clouds, Atmos. Meas. Tech., 5(8), 2039–2055, doi:10.5194/amt-5-2039-2012, 2012b.

Rosenfeld, D., Andreae, M. O., Asmi, A., Chin, M., De Leeuw, G., Donovan, D. P., Kahn, R., Kinne, S., Kiveks, N., Kulmala, M., Lau, W., Schmidt, K. S., Suni, T., Wagner, T., Wild, M. and Quaas, J.: Global observations of aerosol-cloud-precipitation-climate interactions, Rev. Geophys., 52(4), 750–808, doi:10.1002/2013RG000441, 2014a.

Rosenfeld, D., Liu, G., Yu, X., Zhu, Y., Dai, J., Xu, X. and Yue, Z.: High-resolution (375 m) cloud microstructure as seen from the NPP/VIIRS satellite imager, Atmos. Chem. Phys., 14(5), 2479–2496, doi:10.5194/acp-14-2479-2014, 2014b.

Segal, Y., Pinsky, M. and Khain, A.: The role of competition effect in the raindrop formation, Atmos. Res., 83(1), 106–118, doi:10.1016/j.atmosres.2006.03.007, 2007.

Tao, W., Chen, J. and Li, Z.: Impact of aerosols on convective clouds and precipitation, Rev. Geophys.,50, RG2001, doi:10.1029/2011RG000369, 2012.

Twomey, S.: The nuclei of natural cloud formation part II: The supersaturation in natural clouds and the variation of cloud droplet concentration, Geofis. Pura e Appl., 43(1), 243–249, doi:10.1007/BF01993560, 1959.

VanZanten, M., B. Stevens, G. Vali, and D. Lenschow: Observations of drizzle in nocturnal marine stratocumulus, J. Atmos. Sci., 62(1), 88–106, 2005

Voigt, C., Schumann, U., Jurkat, T., Schäuble, D., Schlager, H., Petzold, A., Gayet, J. F., Krämer, M., Schneider, J., Borrmann, S., Schmale, J., Jessberger, P., Hamburger, T., Lichtenstern, M., Scheibe, M., Gourbeyre, C., Meyer, J., Kübbeler, M., Frey, W., Kalesse, H., Butler, T., Lawrence, M. G., Holzäpfel, F., Arnold, F., Wendisch, M., Döpelheuer, A., Gottschaldt, K., Baumann, R., Zöger, M., Sölch, I., Rautenhaus, M. and Dörnbrack, A.: In-situ observations of young contrails–overview and selected results from the CONCERT campaign. *Atmospheric Chemistry and Physics*, *10*(18), 9039-9056, 2010.

Voigt, C., Schumann, U., Jessberger, P., Jurkat, T., Petzold, A., Gayet, J. F., Krmer, M., Thornberry, T. and Fahey, D. W.: Extinction and optical depth of contrails, Geophys. Res. Lett., 38(11), doi:10.1029/2011GL047189, 2011.

Voigt, C., Schumann, U., Minikin, A., Abdelmonem, A., Afchine, A., Borrmann, S., Boettcher, M., Buchholz, B., Bugliaro, L., Costa, A., Curtius, J., Dollner, M., Dörnbrack, A., Dreiling, V., Ebert, V., Ehrlich, A., Fix, A., Forster, L., Frank, F., Fütterer, D., Giez, A., Graf, K., Grooß, J., Groß, S., Heimerl, K., Heinold, B., Hüneke, T., Järvinen, E., Jurkat, T., Kaufmann, S., Kenntner, M., Klingebiel, M., Klimach, T., Kohl, R., Krämer, M., Krisna, T., Luebke, A., Mayer, B., Mertes, S., Molleker, S., Petzold, A., Pfeilsticker, K., Port, M., Rapp, M., Reutter, P., Rolf, C., Rose, D., Sauer, D., Schäfler, A., Schlage, R., Schnaiter, M., Schneider, J., Spelten, N., Spichtinger, P., Stock, P., Walser, A., Weigel, R., Weinzierl, B., Wendisch, M., Werner, F., Wernli, H., Wirth, M., Zahn, A., Ziereis, H. and Zöger, M.: ML-CIRRUS - The airborne experiment on natural cirrus and contrail cirrus with the high-altitude long-range research aircraft HALO, Bull. Am. Meteorol. Soc., doi:10.1175/BAMS-D-15-00213.1, 2017.

Wendisch, M., Pöschl, U., Andreae, M. O., Machado, L. A. T., Albrecht, R., Schlager, H., Rosenfeld, D., Martin, S. T., Abdelmonem, A., Afchine, A., Araùjo, A., Artaxo, P., Aufmhoff, H., Barbosa, H. M. J., Borrmann, S., Braga, R., Buchholz, B., Cecchini, M. A., Costa, A., Curtius, J., Dollner, M., Dorf, M., Dreiling, V., Ebert, V., Ehrlich, A., Ewald, F., Fisch, G., Fix, A., Frank, F., Fütterer, D., Heckl, C., Heidelberg, F., Hüneke, T., Jäkel, E., Järvinen, E., Jurkat, T., Kanter, S., Kästner, U., Kenntner, M., Kesselmeier, J., Klimach, T., Knecht, M., Kohl, R., Kölling, T., Krämer, M., Krüger, M., Krisna, T. C., Lavric, J. V., Longo, K., Mahnke, C., Manzi, A. O., Mayer, B., Mertes, S., Minikin, A., Molleker, S., Münch, S., Nillius, B., Pfeilsticker, K., Pöhlker, C., Roiger, A., Rose, D., Rosenow, D., Sauer, D., Schnaiter, M., Schneider, J., Schulz, C., de Souza, R. A. F., Spanu, A., Stock, P., Vila, D., Voigt, C., Walser, A., Walter, D., Weigel, R., Weinzierl, B., Werner, F., Yamasoe, M. A., Ziereis, H., Zinner, T. and Zöger, M.: The ACRIDICON-CHUVA campaign: Studying tropical deep convective clouds and precipitation over Amazonia using the new German research aircraft HALO, Bull. Am. Meteorol. Soc., 160128144638003, doi:10.1175/BAMS-D-14-00255.1, 2016.

Williams, E.: Contrasting convective regimes over the Amazon: Implications for cloud electrification, J. Geophys. Res., 107(D20), 1–19, doi:10.1029/2001JD000380, 2002.

Figure captions

Figure 1 a) HALO flight tracks during the ACRIDICON-CHUVA experiment. The flight number is indicated at the bottom by colors; b) Flight patterns below and in convective clouds during the ACRIDICON-CHUVA campaign.

Figure 2 a) Precipitation probability as a function of r_e for the CCP-CDP probe for different DWC thresholds (black – DWC > 0.01 g m^{-3}; blue – DWC > 0.02 g m^{-3}; green – DWC > 0.03 g m^{-3}; gold – DWC > 0.05 g m^{-3}; red – DWC > 0.1 g m^{-3}). The dashed line indicates the number of cases (in seconds for each 1-s cloud pass) for each r_e size interval (right axis); b) Similar for the CAS-DPOL probe.

Figure 3 Cloud droplet effective radius (r_e) calculated from the CCP-CDP data versus r_e calculated from the CAS-DPOL data for all flights shown in Figure 1a.

Figure 4 a) Droplet mean volume radius versus cloud droplet effective radius (r_e) for 1-Hz averaged droplet size distributions from CCP-CDP measured during various flights over the Amazon; b) similar for CAS-DPOL. The color-coding denotes different flights over the Amazon. The number of measurements that were used to calculate the linear best fit for each location is denoted by “n” in the legend. The r_e and r_v mean linear relationship for all flights is shown below the linear relationship for each flight in black color.

Figure 5 Cloud droplet concentration measured with CCP-CDP as a function of temperature for flight AC07. Each dot indicates a 1-Hz average concentration. The sample number (N) and the approximate start time of the cloud profile are shown at the top of the panel.

Figure 6 a) Mean cloud droplet size distribution calculated from the CCP-CDP data for a cloud pass at cloud base during flight AC07. The flight number, initial time of cloud pass, and duration in seconds are shown at the top of graph. The mean total number of droplets (N_{dmean}), the maximum total number of droplets (N_{dmax}) in one second for this cloud pass, and the approximate height (H) and temperature (T) are shown at the upper-right corner of the graph; b) Cloud droplet effective radius (r_e) calculated from CCP-CDP as a function of temperature indicated with dots. The black line indicates the estimated adiabatic effective radius (r_{ea}) as a function of temperature.

Figure 7a-c. Droplet size distribution composite from the CCP-CDP and CCP-CIP probes (left panel). Similar for indicated cloud water content (CWC) in the right panel. Indicated at the top of the panels are the HALO flight number, date, time of flight (UTC), duration of cloud pass in seconds, temperature (T) and altitude (H) above sea level, and the mean values for the total number of droplets (N_d), CWC, DWC, RWC, and r_e. The color bars indicate the height of HALO during the cloud pass. On the right side of the panels CCP-CIP images corresponding to the cloud pass are shown.

Figure 8 Image taken from the HALO cockpit just before the aircraft penetration of a convective cloud with lightning activity during flight AC07. In this case, the cloud pass height was 9,022 m (temperature ~ -25 ºC) and the maximum CWC measured was 0.55 g m^{-3}.

Figure 9 a) Cloud droplet effective radius (r_e) as a function of cloud depth (D_c) for flight AC07. The line indicates the r_e estimated for adiabatic growth (r_{ea}) from cloud base (dashed lines indicate the r_{ea} values considering the uncertainty of the estimate). The height of 0 ºC is indicated by a black horizontal bar across the r_{ea} line. The estimated adiabatic number of droplets (N_a) at cloud base is shown at the top of the figure. b) Similar to a) for Cloud water content (adiabatic values are shown by lines).

Figure 10 a) Cloud droplet concentrations measured with the CCP-CDP as a function of temperature for flight AC19. Each dot indicates 1Hz average concentration. The sample number in seconds (N) and the start time of the cloud profile are shown at the top of the panel; b) Similar to Figure 9 for flight AC19.

Figures 11 a-b) Similar to Figures 7a-c for flight AC19.

Figure 12 Cumulative aerosol size distribution below cloud base calculated from the PCASP probe for typical clean, polluted, and very polluted regions (solid line) for flights AC12 (very polluted), AC18 (polluted), and AC19 (clean). Similar for cumulative cloud droplet size distribution calculated with CCP-CDP (dashed line). The flight numbers are indicated by colors at the top of the panel.

Figure 13 a) Cloud droplet concentrations measured with the CCP-CDP as a function of temperature for flight AC09. Each dot indicates 1-Hz average concentration. The sample number in seconds (N) and the start time of the cloud profile are shown at the top of the panel; b) Similar to Figure 9 for flight AC09.

Figures 14 a-b) Similar to Figures 7a-c for flight AC09.

Figure 15 a) Cloud droplet concentration measured with the CCP-CDP probe as a function of temperature for flight AC13. Each dot indicates a 1-Hz average concentration. The sample number and the approximate time of the cloud profile are shown at the top of the panel; b) Similar to figure 9 for Flight AC13.

Figures 16 Similar to Figures 7a-c for flight AC13.

Figure 17. Cloud depth (D_c) as a function of the estimated adiabatic number of droplets (N_a) at cloud base. D_c for adiabatic cloud droplet effective radius (r_{ea}) equal 13 µm (or D_{13}) are indicated by triangles. Similar for cloud depth of rain initiation (D_r) [indicated by circles] and cloud depth for ice initiation (D_i) [indicated by asterisk]. The flight numbers are indicated by colors on the right side of the panel. The values of D_{13}, D_r, and D_i are shown in Table 1. The black line indicates the linear equation for D_{13} as a function of N_a for all flights, where: $D_{13} = (5 \pm 0.7) \cdot N_a$.

Figure 18 CDP-measured cloud droplet effective radius (r_e) (colored dots) and estimated cloud droplet adiabatic effective radius (r_{ea}) (colored lines) as a function of cloud depth (D_c) for all flights (indicated by colors). The height of 0 ºC is indicated by a horizontal bar across the r_{ea} line. The circles indicate the approximate values of drizzle water content (DWC) calculated from the CCP-CIP data, the range of DWC values is indicated in the table at the upper-right side of the figure. The star symbols indicate approximate mixed phase drizzle water content (MPWC) values calculated from the CCP-CIP data (indicated in the table at the bottom-right side of the figure). The temperature in ºC of rain or ice initiation (D_r and D_i, respectively) is indicated by colored numbers close to the circle or star symbols.

Table captions

Table 1. List of abbreviations and symbols.

Table 2. Description of cloud probes, size range intervals and hydrometeor shapes observed on CCP-CIP images used to calculate CWC, DWC, RWC and MPWC.

Table 3. Classification of each flight as a function of N_a at cloud base. The values of cloud base height (*Cbh*) and temperature (*T*), D_{13}, D_r and D_i in m and temperatures in ºC are also shown for convective cloud measurements of each flight.

Tables

Table 1. List of abbreviations and symbols.

Abbreviation/notation	Description	Units
ACRIDICON-CHUVA	Aerosol, Cloud, Precipitation, and Radiation Interactions and Dynamics of Convective Cloud Systems - CHUVA (Cloud processes of tHe main precipitation systems in Brazil: A contribUtion to cloud resolVing modeling and to the GPM [Global Precipitation Measurements])	-
CAS-DPOL	Cloud and Aerosol Spectrometer	-
Cbh	Cloud base height	m
CCP-CDP	Cloud Combination Probe - Cloud Droplet Probe	-
CCP-CIP	Cloud Combination Probe - Cloud Imaging Probe	-
CCN	Cloud Condensation Nuclei	cm^{-3}
CWC	Cloud water content	$g\ m^{-3}$
CWC_a	Adiabatic cloud water content	$g\ m^{-3}$
D_c	Cloud depth - distance from cloud base	m
D_r	Cloud depth where first drizzle with drop shape was detected	m
D_i	Cloud depth where first drizzle with ice shape was detected	m
DWC	Drizzle Water Content	$g\ m^{-3}$
DSD	Cloud-droplet size distribution	$cm^{-3}\ \mu m^{-1}$
D_{13}	Cloud depth where r_{ea} = 13 µm	m
IN	Ice Nuclei	cm^{-3}
K	The collection kernel of a pair of droplets	$cm^{-3}\ s^{-1}$
MPWC	Mixed Phase Water Content	$g\ m^{-3}$
M_v	Mean volume cloud droplet	μm^{-3}
M_{va}	Adiabatic mean volume cloud droplet	μm^{-3}
N_d	Number concentration of droplets	cm^{-3}
N_a	Adiabatic number concentration of droplets	cm^{-3}
PCASP	Passive Cavity Aerosol Spectrometer Probe	-
PSD	Aerosol particle size distribution	$cm^{-3}\ \mu m^{-1}$
r_e	The effective radius of the cloud droplet spectra	µm
r_{ea}	The adiabatic effective radius of the cloud droplet spectra	µm
r_v	The mean volume radius of the cloud droplets	µm
RWC	Rainwater Content	$g\ m^{-3}$
S	Supersaturation	%
T	Temperature	ºC
W	Vertical velocity	$m\ s^{-1}$

Table 2. Description of cloud probes, size range intervals and hydrometeor shapes observed on CCP-CIP images used to calculate CWC, DWC, RWC and MPWC.

Abbreviation/Notation	Instrument	Size range	Hydrometeor shapes
CWC	CCP-CDP/CAS-DPOL	3-50 µm	Cloud droplets
DWC	CCP-CIP	75-250 µm	Cloud droplets and raindrops
RWC	CCP-CIP	250-960 µm	Cloud droplets and raindrops
MPWC	CCP-CIP	75-960 µm	Cloud droplets and ice particles

Table 3. Classification of each flight as a function of N_a at cloud base. The values of cloud base height (*Cbh*) and temperature (*T*), D_{13}, D_r and D_i in m and temperatures in ºC are also shown for convective cloud measurements of each flight.

Flight	*Cbh* (m)/ *T* (ºC)	N_a (cm^{-3})	D_{13} (m)	D_r (m)	*T*(ºC)	D_i (m)	*T*(ºC)	Classification
AC07	1900 / 16	963	4500	-	-	4537	-9.1	very polluted
AC08	1100 / 20	920	3900	-	-	-	-	very polluted
AC09	1200 / 19.5	566	2400	3000	2.4	5217	-9.2	polluted
AC12	2200 / 15.5	1546	9000	-	-	-	-	very polluted
AC13	2200 / 15.5	1080	5500	-	-	4800	-14.1	very polluted
AC18	1700 / 17	666	2900	3800	-5.7	-	-	polluted
AC19	600 / 22	276	1000	1660	10	-	-	clean
AC20	1900 / 16.5	987	5000	-	-	-	-	very polluted

Figures

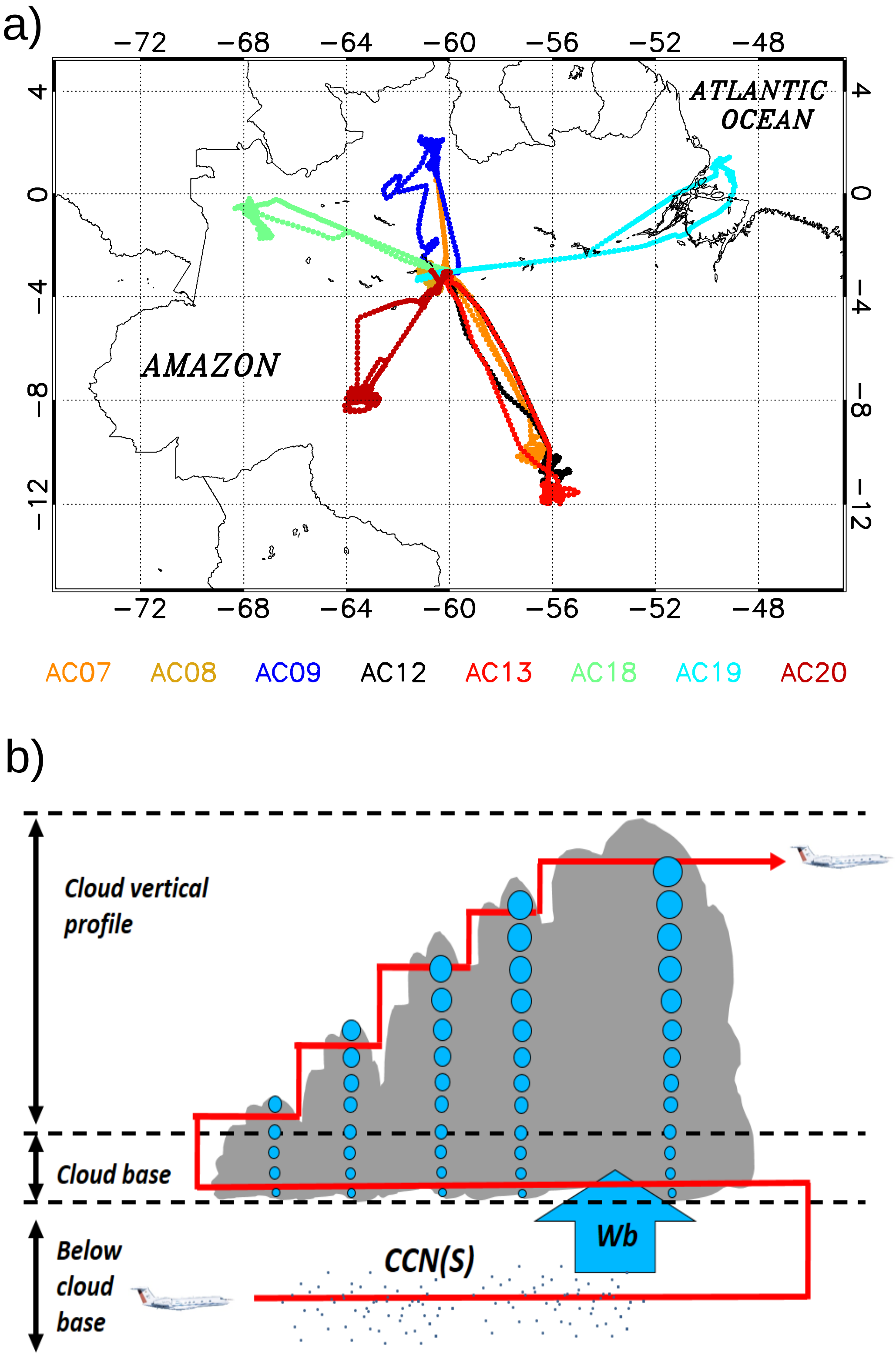

Figure 1 a) HALO flight tracks during the ACRIDICON-CHUVA experiment. The flight number is indicated at the bottom by colors; b) Flight patterns below and in convective clouds during the ACRIDICON-CHUVA campaign.

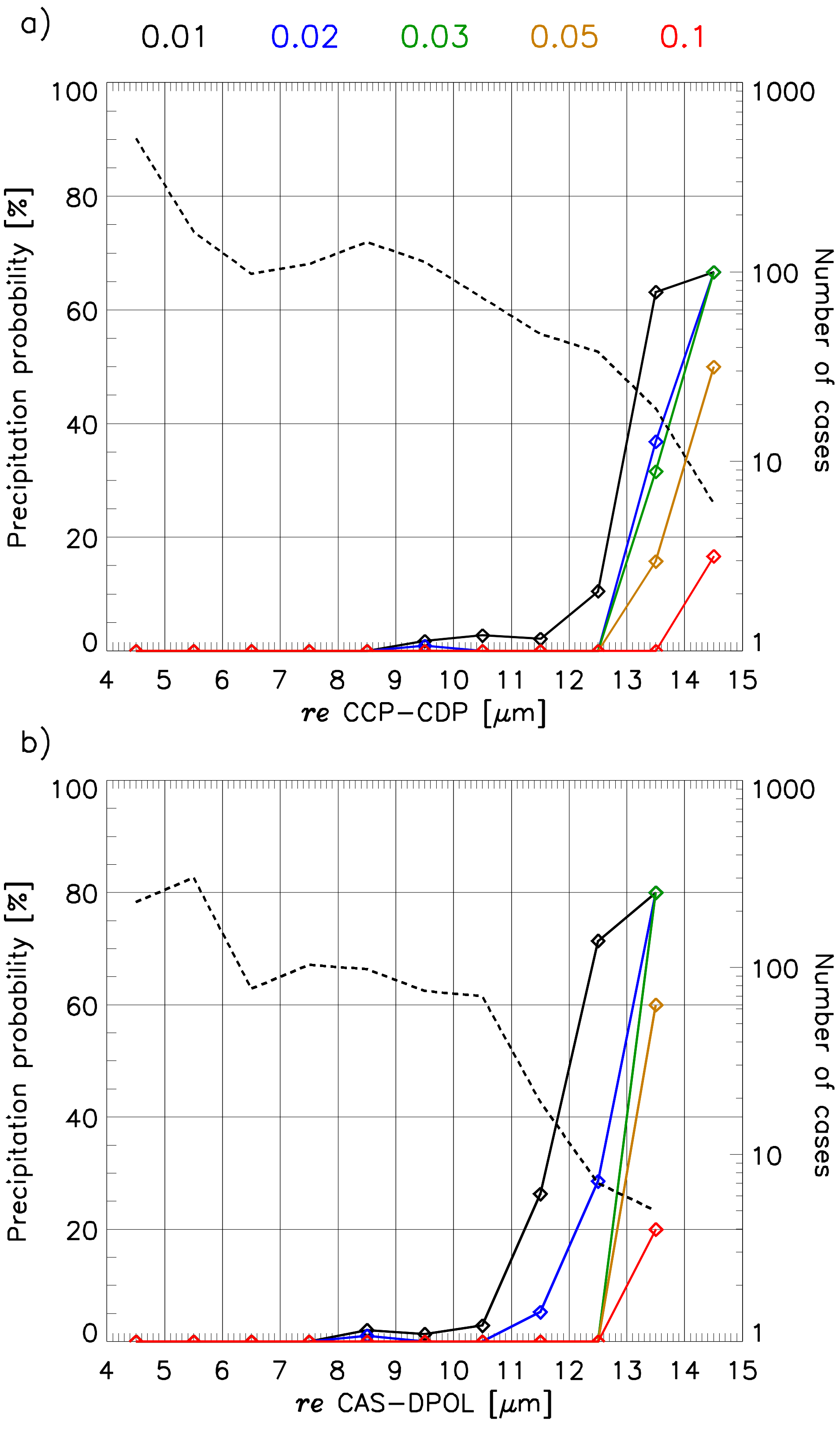

875

Figure 2 a) Precipitation probability as a function of r_e for the CCP-CDP probe for different DWC thresholds (black – DWC > 0.01 g m^{-3}; blue – DWC > 0.02 g m^{-3}; green – DWC > 0.03 g m^{-3}; gold – DWC > 0.05 g m^{-3}; red – DWC > 0.1 g m^{-3}). The dashed line indicates the number of cases (in seconds for each 1-s cloud pass) for each r_e size interval (right axis); b) Similar for the CAS-DPOL probe.

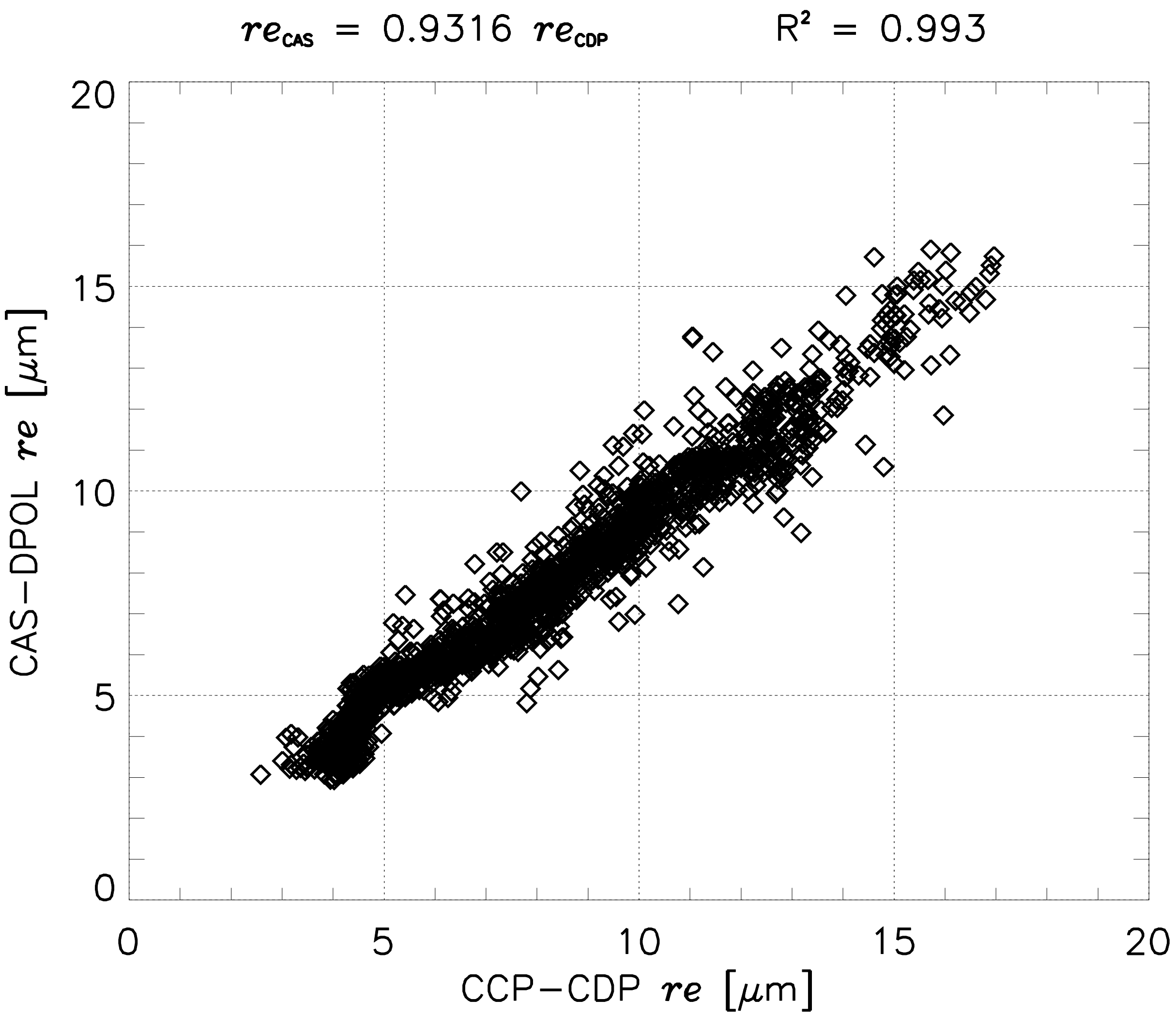

880

Figure 3 Cloud droplet effective radius (r_e) calculated from the CCP-CDP data versus r_e calculated from the CAS-DPOL data for all flights shown in Figure 1a.

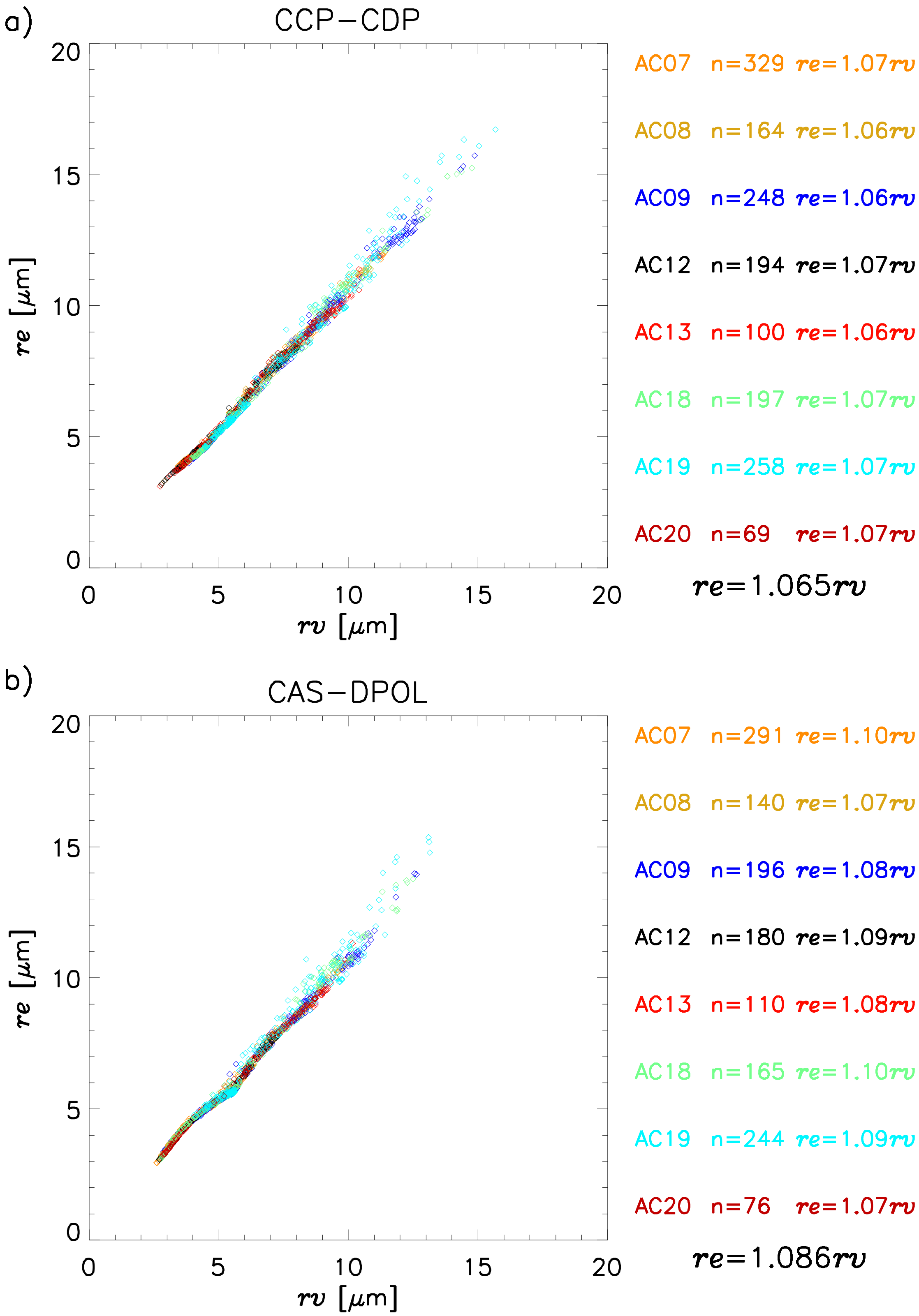

Figure 4 a) Droplet mean volume radius versus cloud droplet effective radius (r_e) for 1-Hz averaged droplet size distributions from CCP-CDP measured during various flights over the Amazon; b) similar for CAS-DPOL. The color-coding denotes different flights over the Amazon. The number of measurements that were used to calculate the linear best fit for each location is denoted by "n" in the legend. The r_e and r_v mean linear relationship for all flights is shown below the linear relationship for each flight in black color.

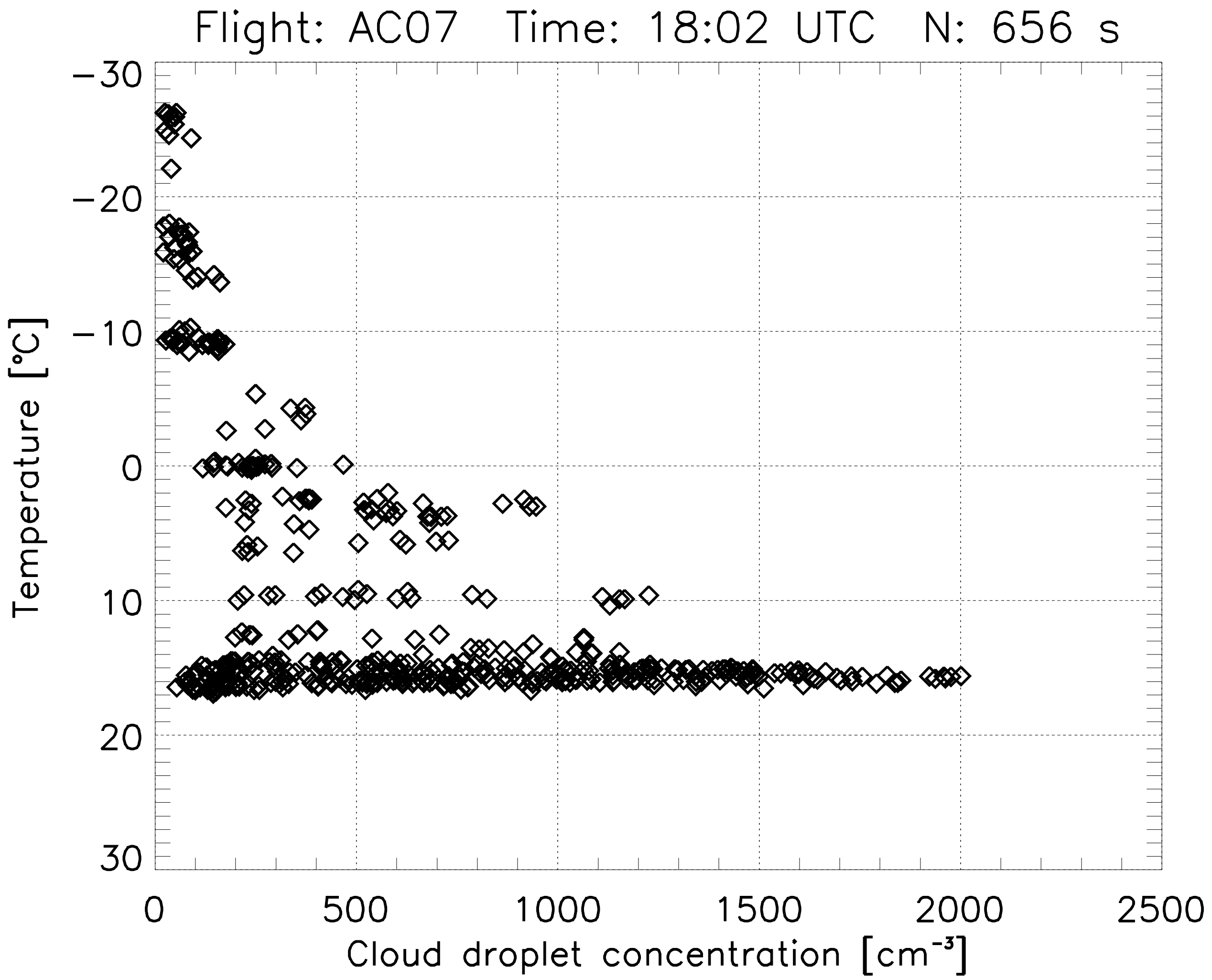

Figure 5 Cloud droplet concentration measured with CCP-CDP as a function of temperature for flight AC07. Each dot indicates a 1-Hz average concentration. The sample number (N) and the approximate start time of the cloud profile are shown at the top of the panel.

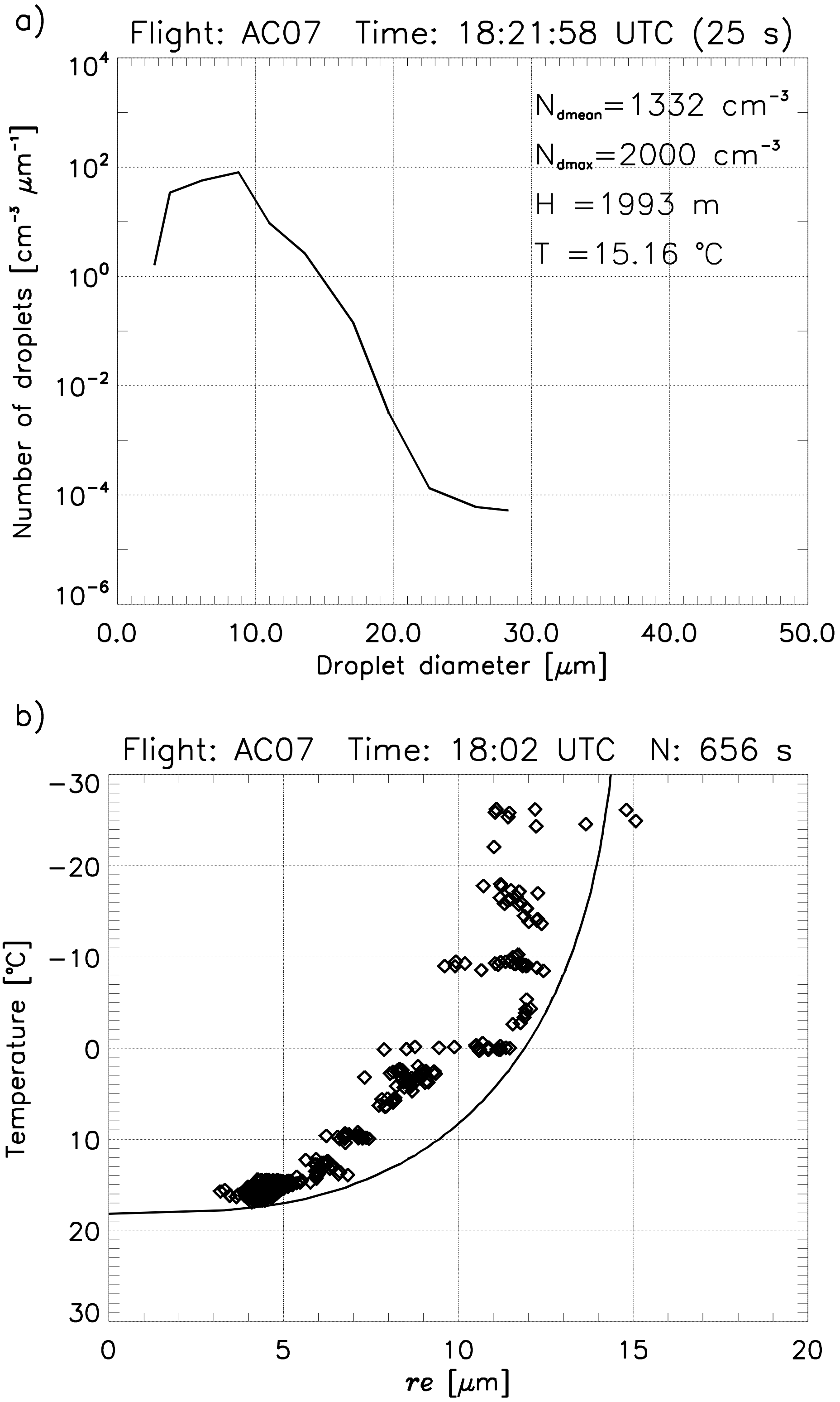

Figure 6 a) Mean cloud droplet size distribution calculated from the CCP-CDP data for a cloud pass at cloud base during flight AC07. The flight number, initial time of cloud pass, and duration in seconds are shown at the top of graph. The mean total number of droplets (N_{dmean}), the maximum total number of droplets (N_{dmax}) in one second for this cloud pass, and the approximate height (H) and temperature (T) are shown at the upper-right corner of the graph; b) Cloud droplet effective radius (r_e) calculated from CCP-CDP as a function of temperature indicated with dots. The black line indicates the estimated adiabatic effective radius (r_{ea}) as a function of temperature.

a)

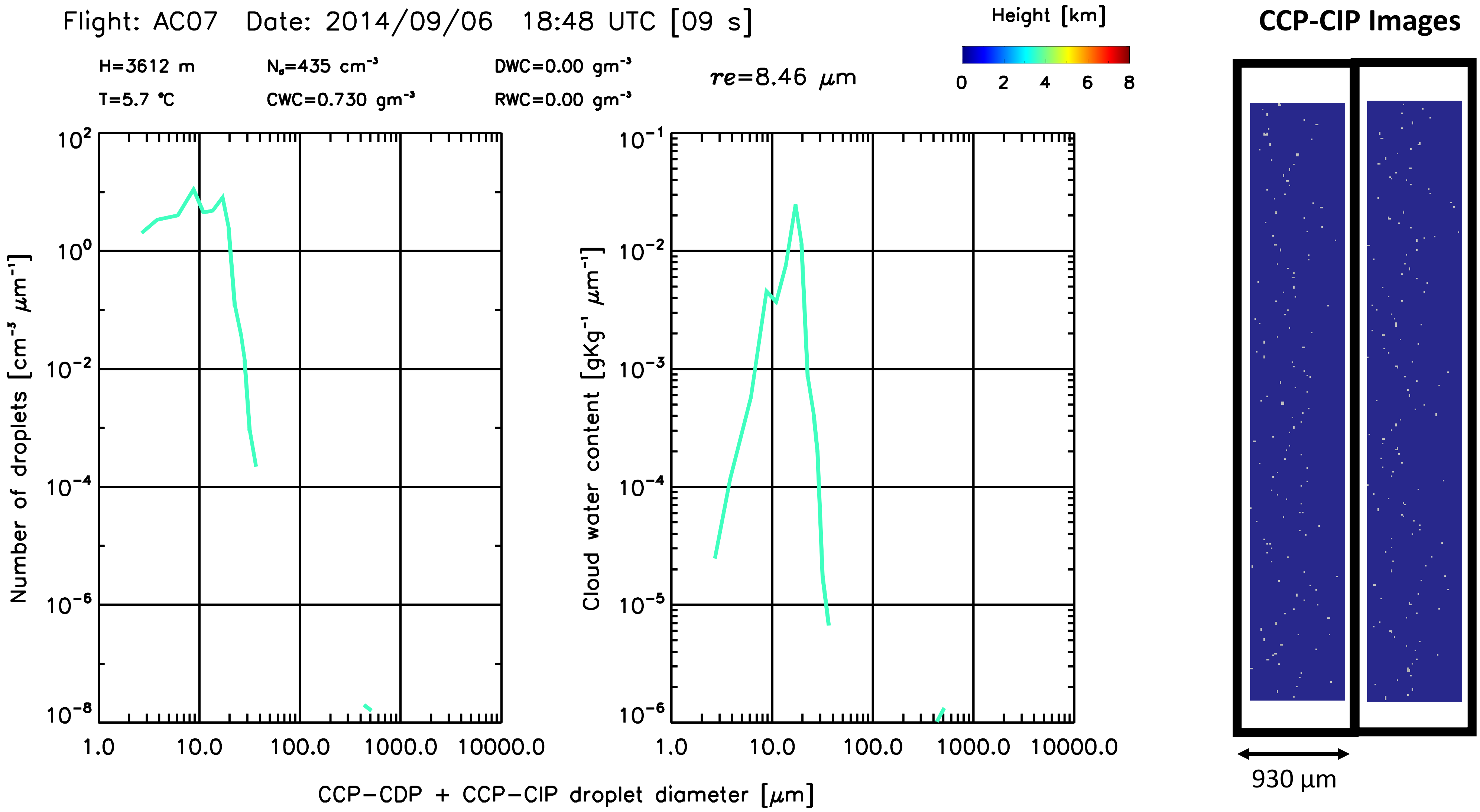

Flight: AC07 Date: 2014/09/06 18:48 UTC [09 s]
H=3612 m
T=5.7 °C
N_d=435 cm^-3
CWC=0.730 gm^-3
DWC=0.00 gm^-3
RWC=0.00 gm^-3
re=8.46 μm
Height [km]
0 2 4 6 8
Number of droplets [cm^-3 μm^-1]
Cloud water content [gKg^-1 μm^-1]
CCP−CDP + CCP−CIP droplet diameter [μm]
1.0 10.0 100.0 1000.0 10000.0
CCP-CIP Images
930 μm

b)

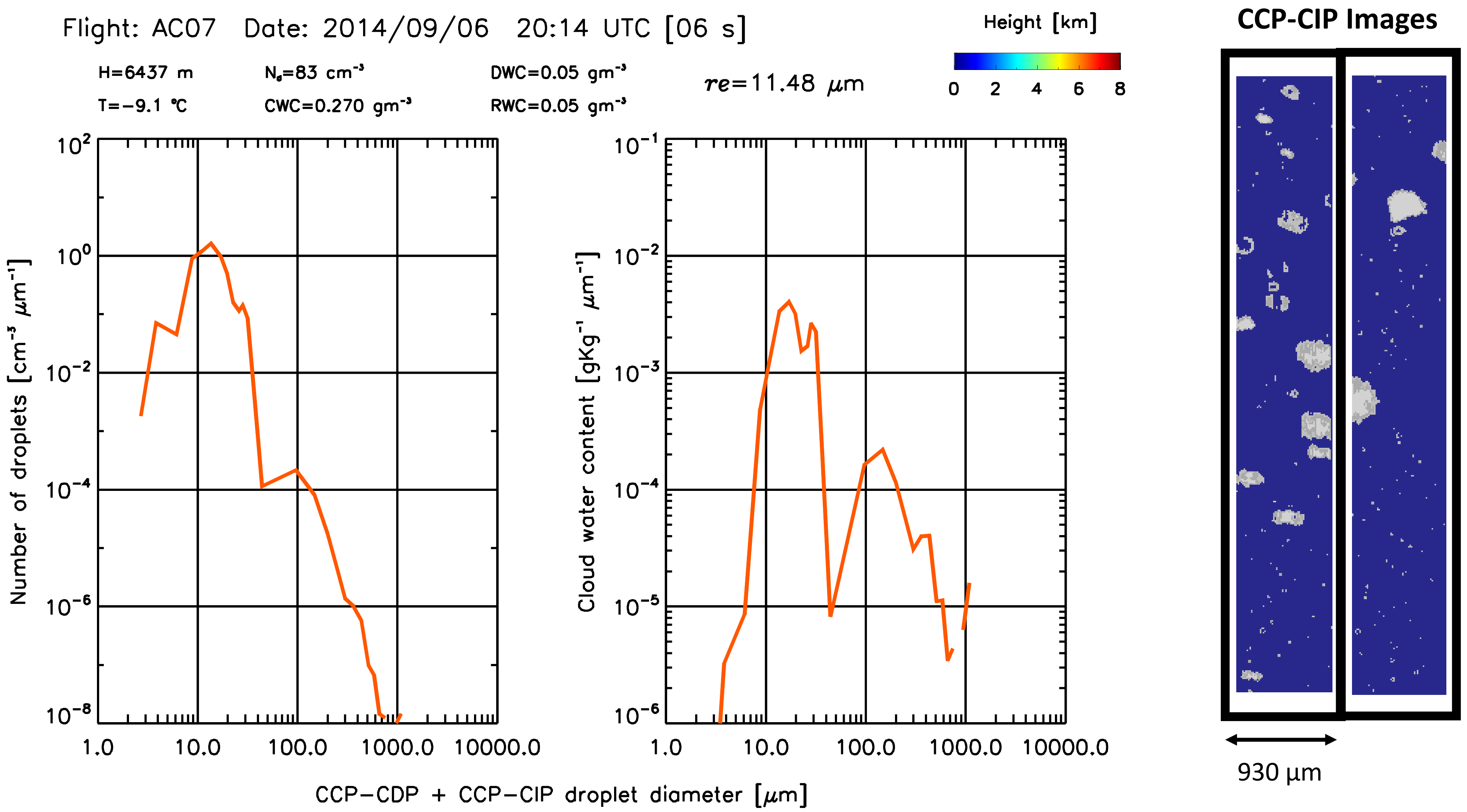

Flight: AC07 Date: 2014/09/06 20:14 UTC [06 s]
H=6437 m
T=−9.1 °C
N$_d$=83 cm^{-3}
CWC=0.270 gm^{-3}
DWC=0.05 gm^{-3}
RWC=0.05 gm^{-3}
re=11.48 μm
Height [km]
0 2 4 6 8
Number of droplets [cm^{-3} μm^{-1}]
10^{2} 10^{0} 10^{-2} 10^{-4} 10^{-6} 10^{-8}
Cloud water content [gKg^{-1} μm^{-1}]
10^{-1} 10^{-2} 10^{-3} 10^{-4} 10^{-5} 10^{-6}
1.0 10.0 100.0 1000.0 10000.0
CCP−CDP + CCP−CIP droplet diameter [μm]
CCP-CIP Images
930 μm

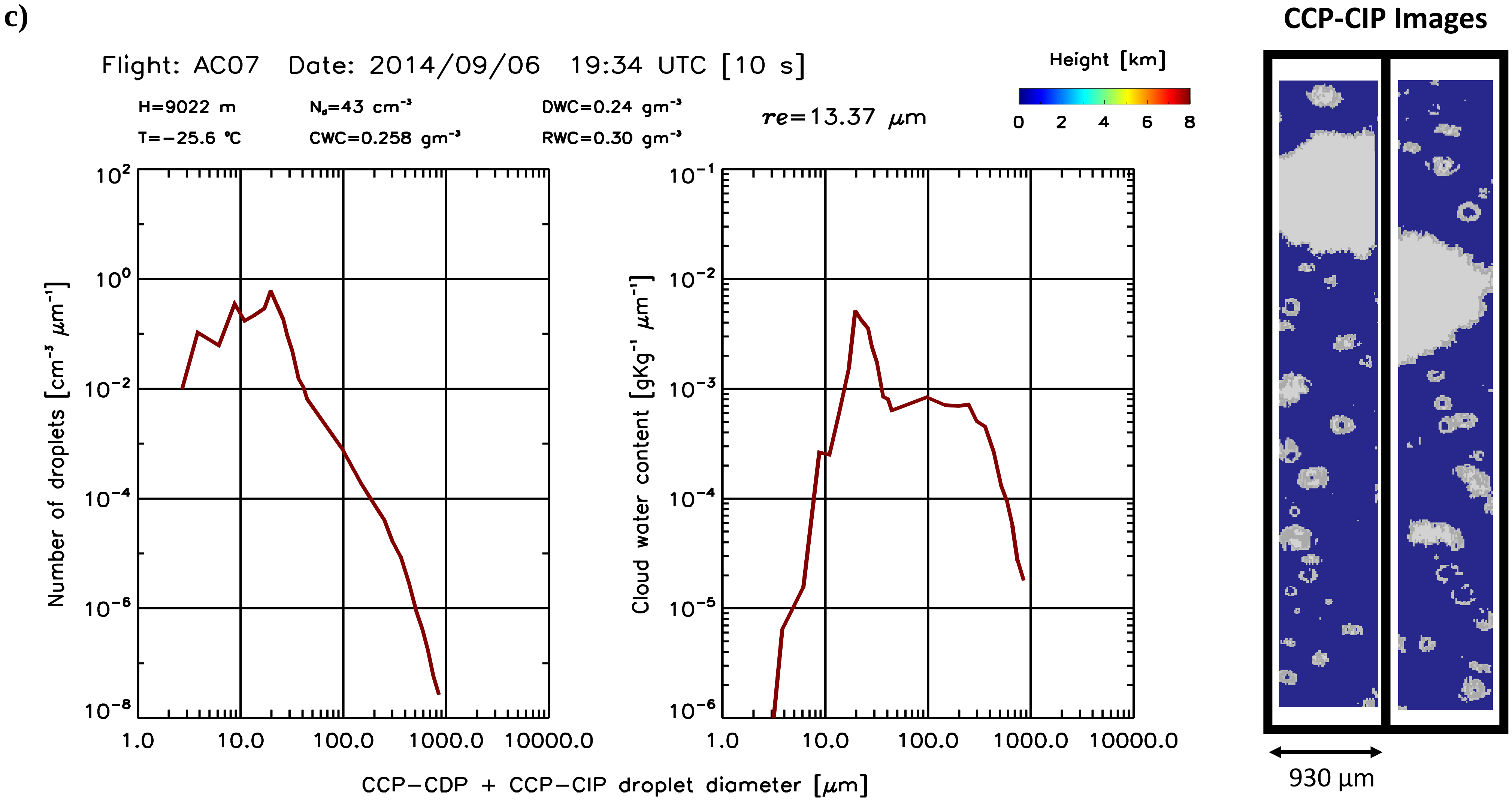

Figure 7a-c. Mean droplet size distribution composite from the CCP-CDP and CCP-CIP probes (left panel). Similar for indicated cloud water content in the right panel. Indicated at the top of the panels are the HALO flight number, date, time of flight (UTC), duration of cloud pass in seconds, temperature (T) and altitude (H) above sea level, and the mean values for the total number of droplets (N_d), CWC, DWC, RWC, and r_e. The color bars indicate the height of HALO during the cloud pass. On the right side of the panels CCP-CIP images corresponding to the cloud pass are shown.

Figure 8 Image taken from the HALO cockpit just before the aircraft penetration of a convective cloud with lightning activity during flight AC07. In this case, the cloud pass height was 9,022 m (temperature ~ -25 ºC) and the maximum CWC measured was 0.55 g m^{-3}.

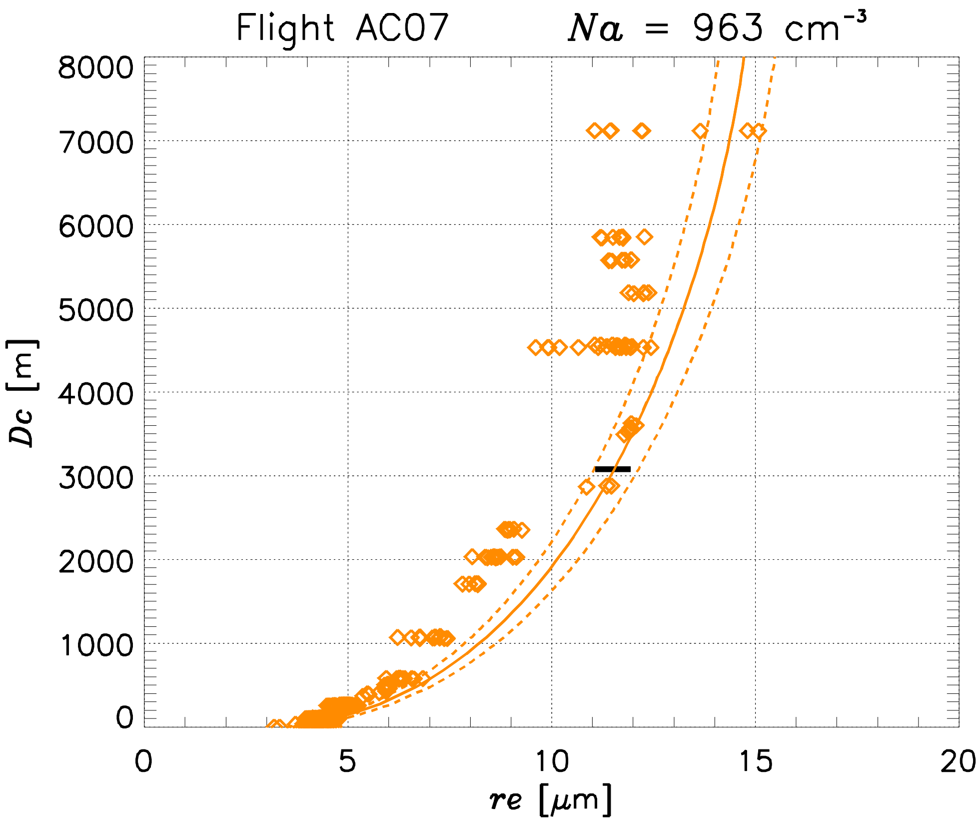

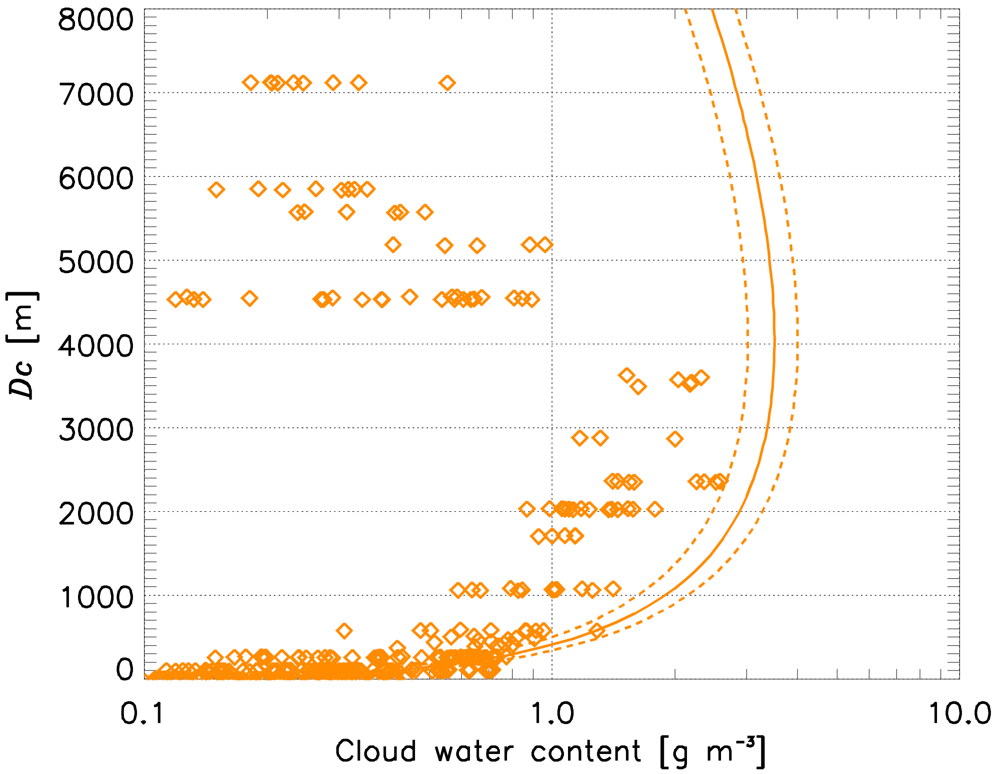

Figure 9 a) Cloud droplet effective radius (r_e) as a function of cloud depth (D_c) for flight AC07. The line indicates the r_e estimated for adiabatic growth (r_{ea}) from cloud base (dashed lines indicate the r_{ea} values considering the uncertainty of the estimate). The height of 0 °C is indicated by a black horizontal bar across the r_{ea} line. The estimated adiabatic number of droplets (N_a) at cloud base is shown at the top of the figure. b) Similar to a) for Cloud water content (adiabatic values are shown by lines).

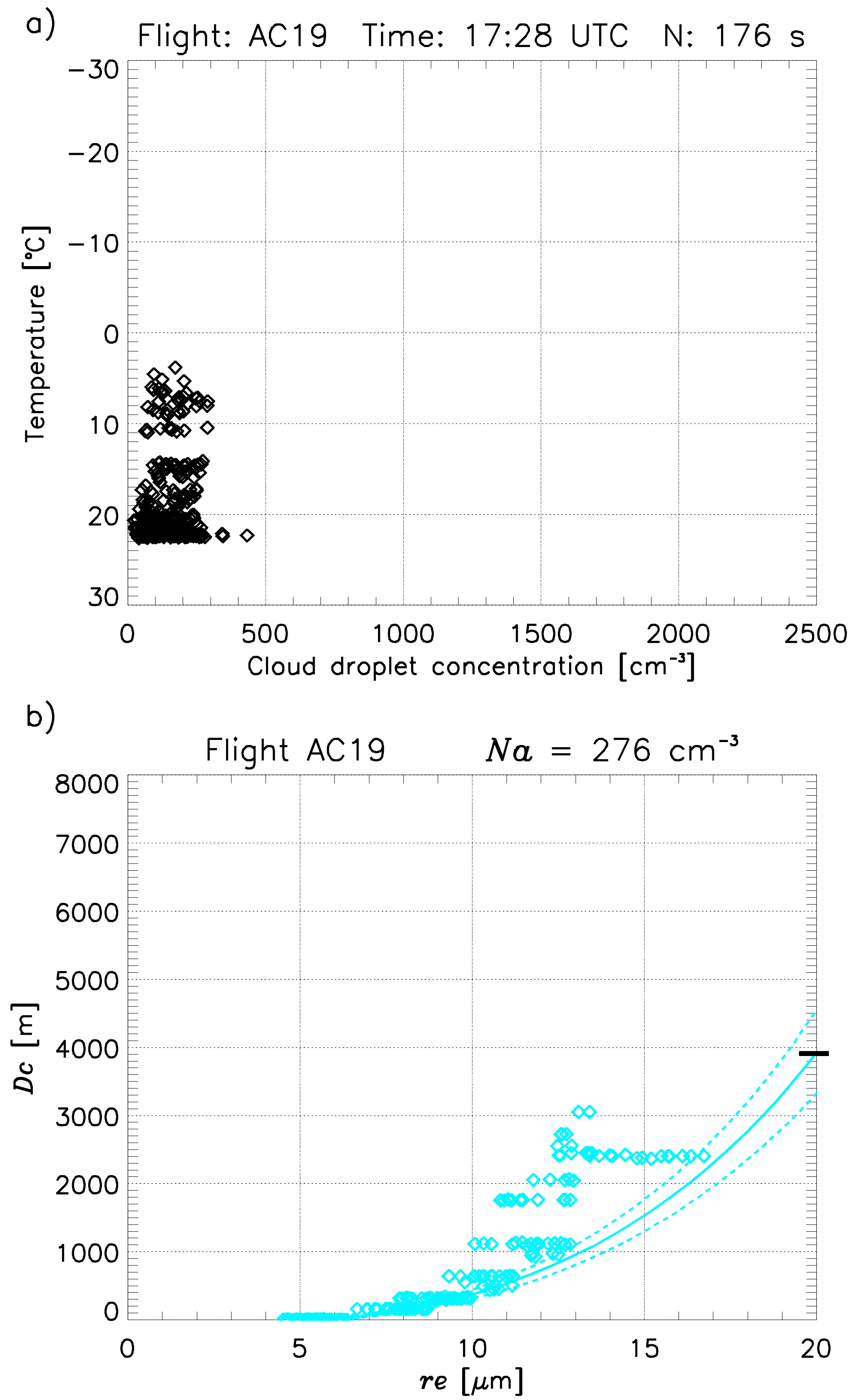

Figure 10 a) Cloud droplet concentrations measured with the CCP-CDP as a function of temperature for flight AC19. Each dot indicates 1Hz average concentration. The sample number in seconds (N) and the start time of the cloud profile are shown at the top of the panel; b) Similar to Figure 9 for flight AC19.

a)

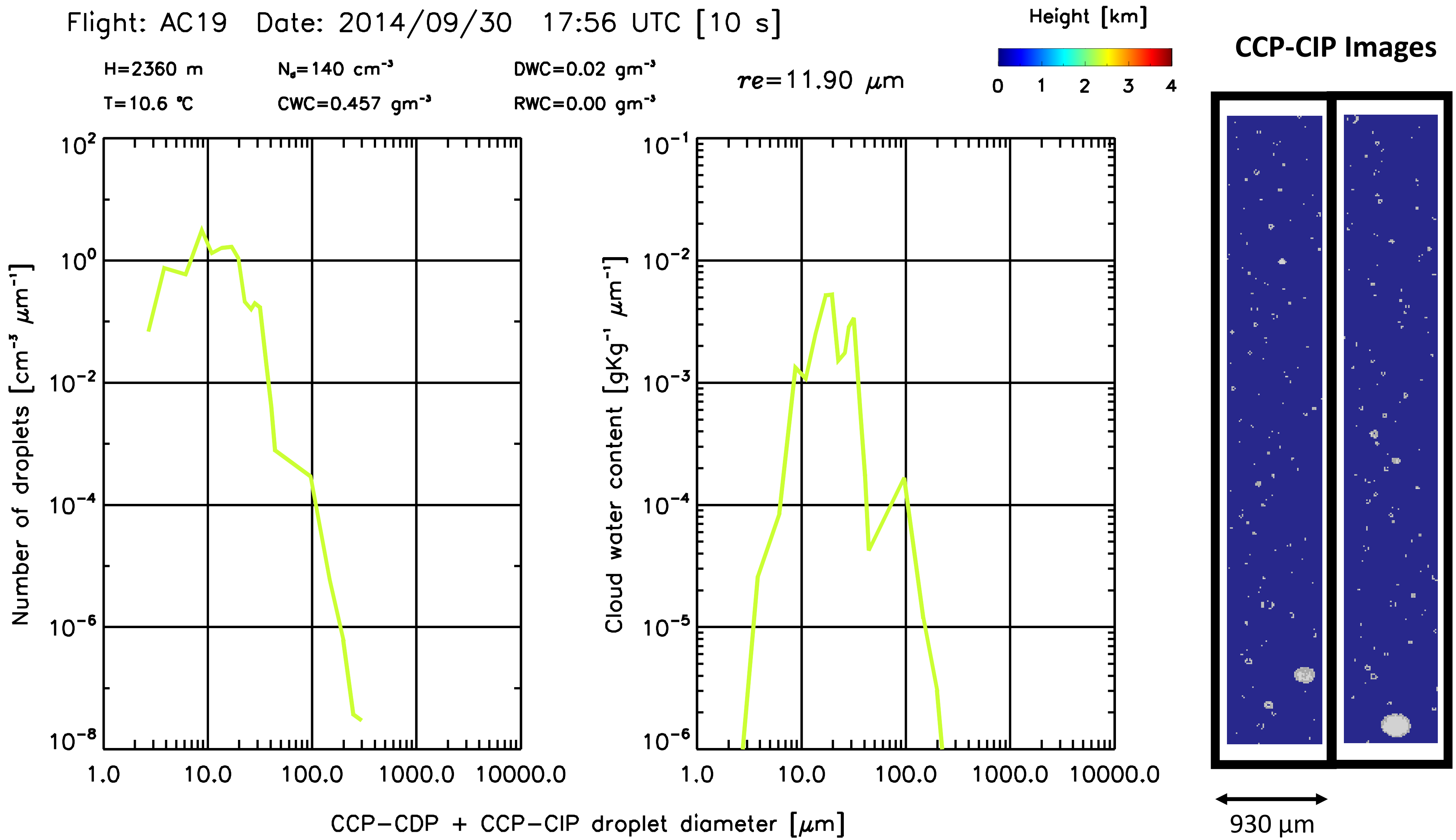
Flight: AC19 Date: 2014/09/30 17:56 UTC [10 s]
H=2360 m
T=10.6 °C
N_d=140 cm^{-3}
CWC=0.457 gm^{-3}
DWC=0.02 gm^{-3}
RWC=0.00 gm^{-3}
re=11.90 μm
Height [km]
0 1 2 3 4
CCP-CIP Images
Number of droplets [cm^{-3} μm^{-1}]
Cloud water content [gKg^{-1} μm^{-1}]
1.0 10.0 100.0 1000.0 10000.0
CCP−CDP + CCP−CIP droplet diameter [μm]
930 μm

b)

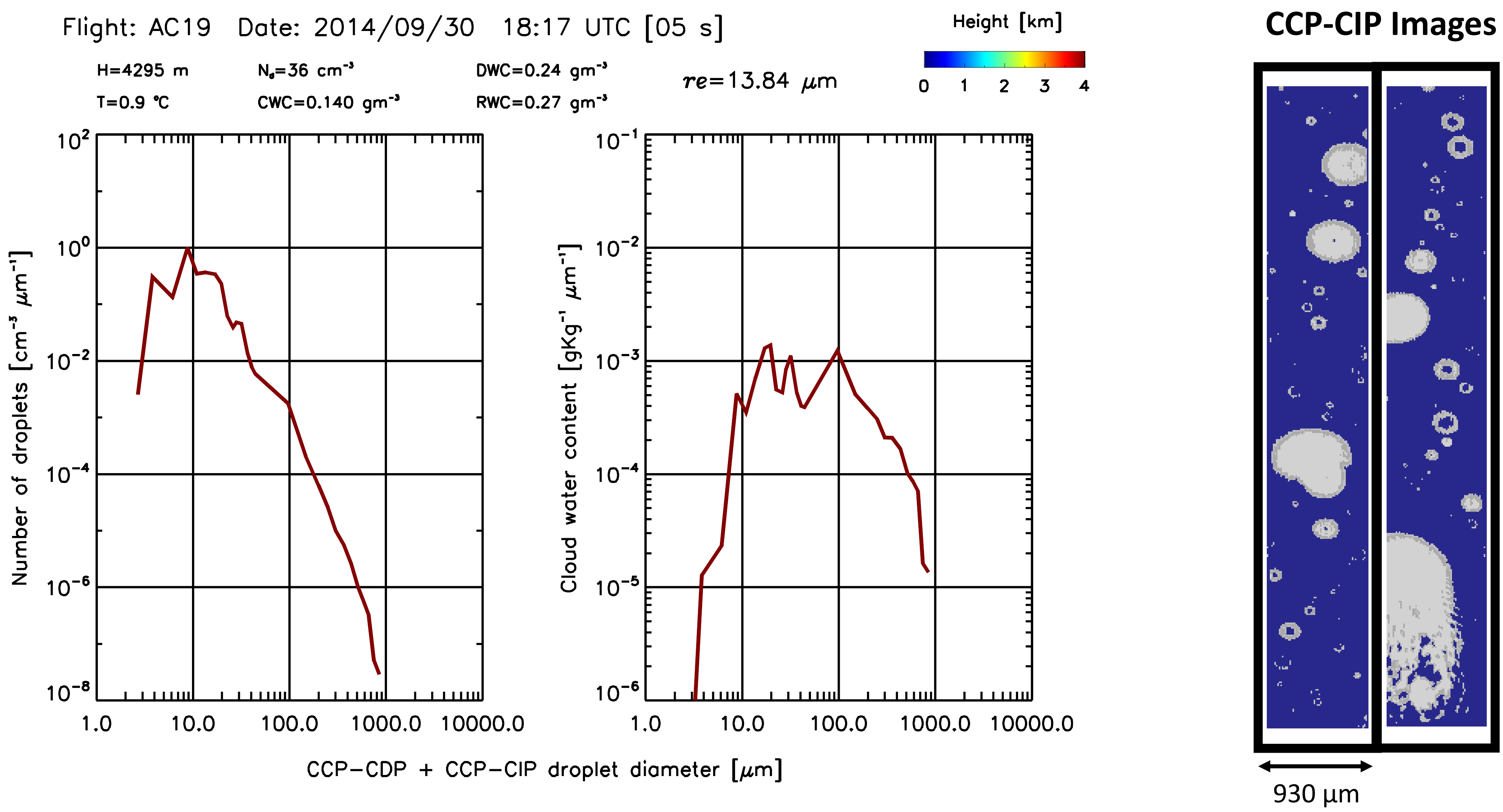

Figures 11 a-b) Similar to Figures 7a-c for flight AC19.

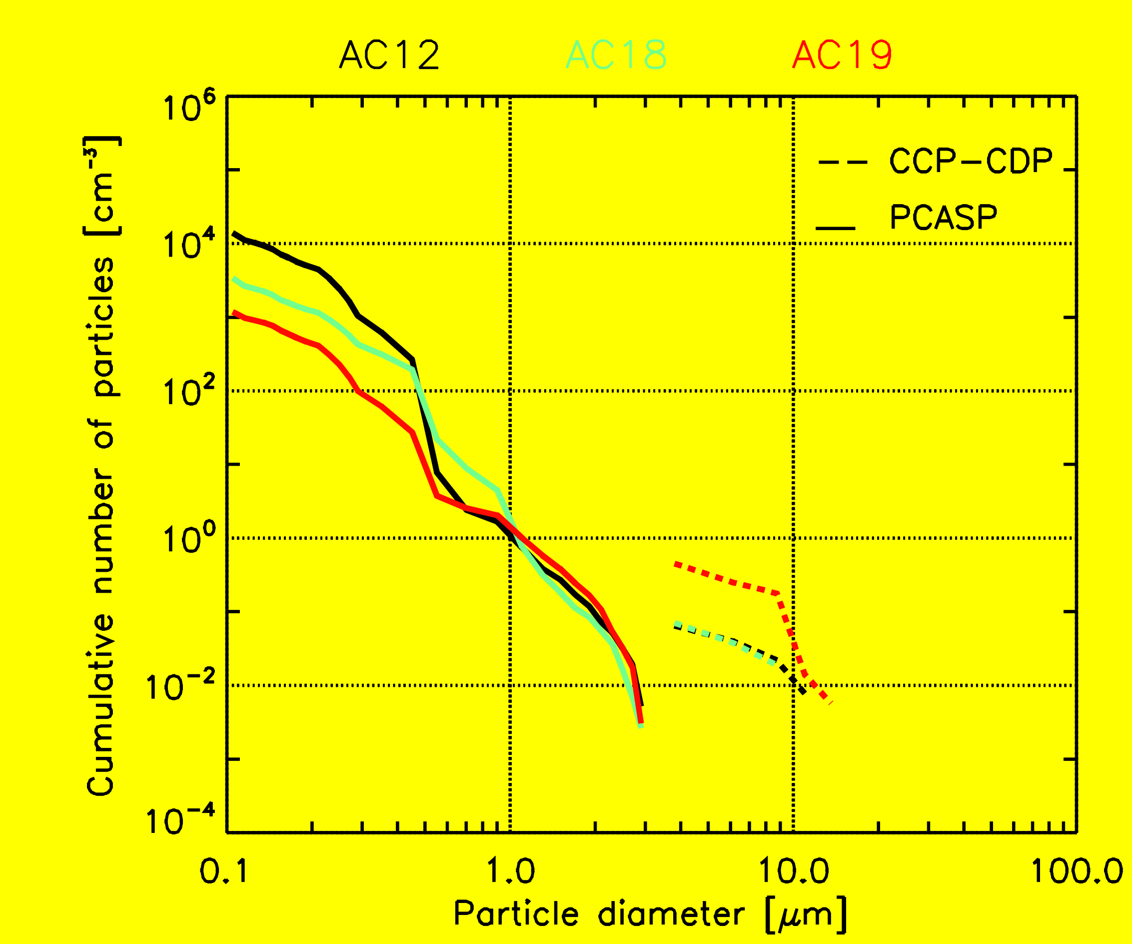

Figure 12 Cumulative aerosol size distribution below cloud base calculated from the PCASP probe for typical clean, polluted, and very polluted regions (solid line) for flights AC12 (very polluted), AC18 (polluted), and AC19 (clean). Similar for cumulative cloud droplet size distribution calculated with CCP-CDP (dashed line). The flight numbers are indicated by colors at the top of the panel.

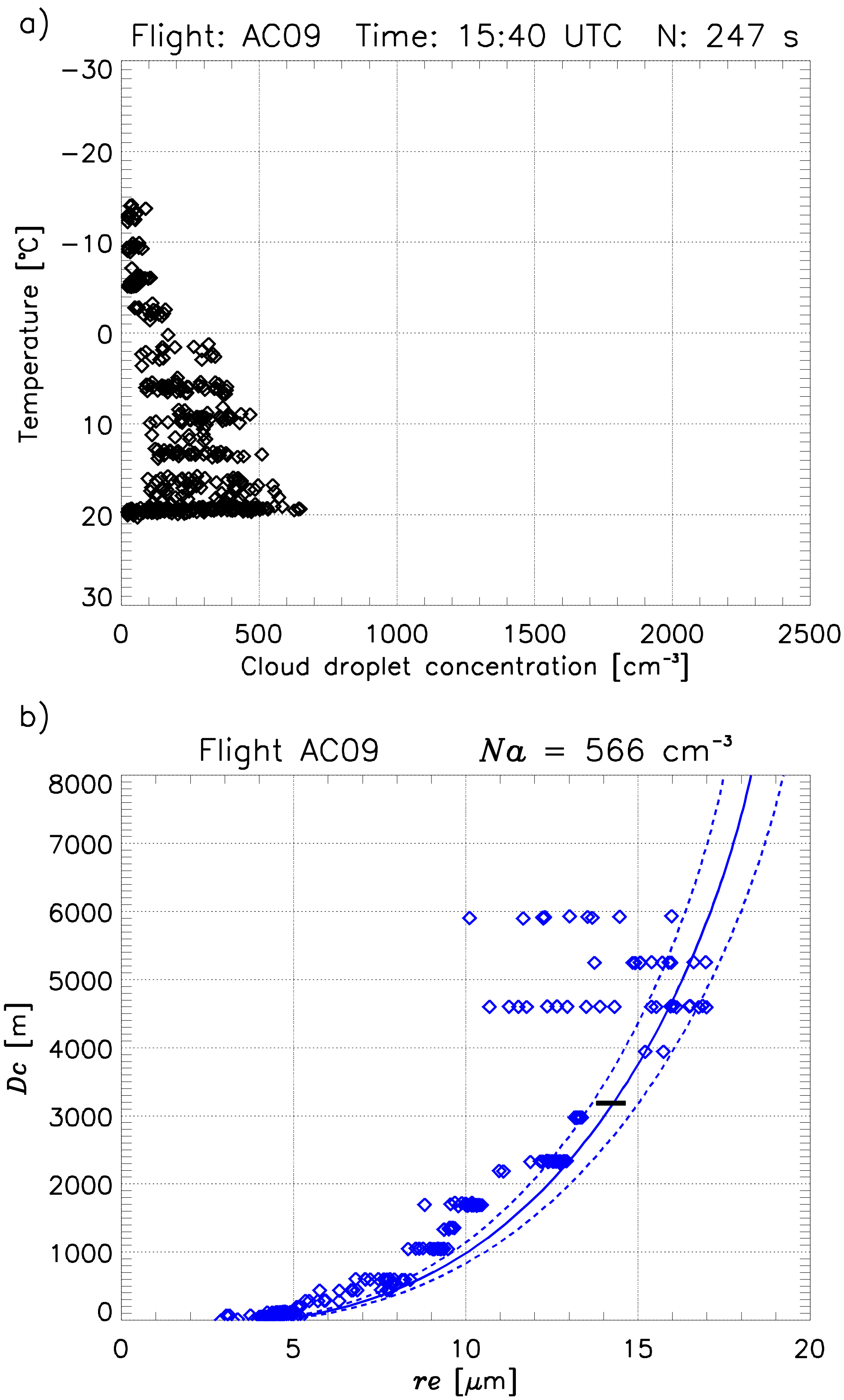

Figure 13 a) Cloud droplet concentrations measured with the CCP-CDP as a function of temperature for flight AC09. Each dot indicates 1-Hz average concentration. The sample number in seconds (N) and the start time of the cloud profile are shown at the top of the panel; b) Similar to Figure 9 for flight AC09.

a)

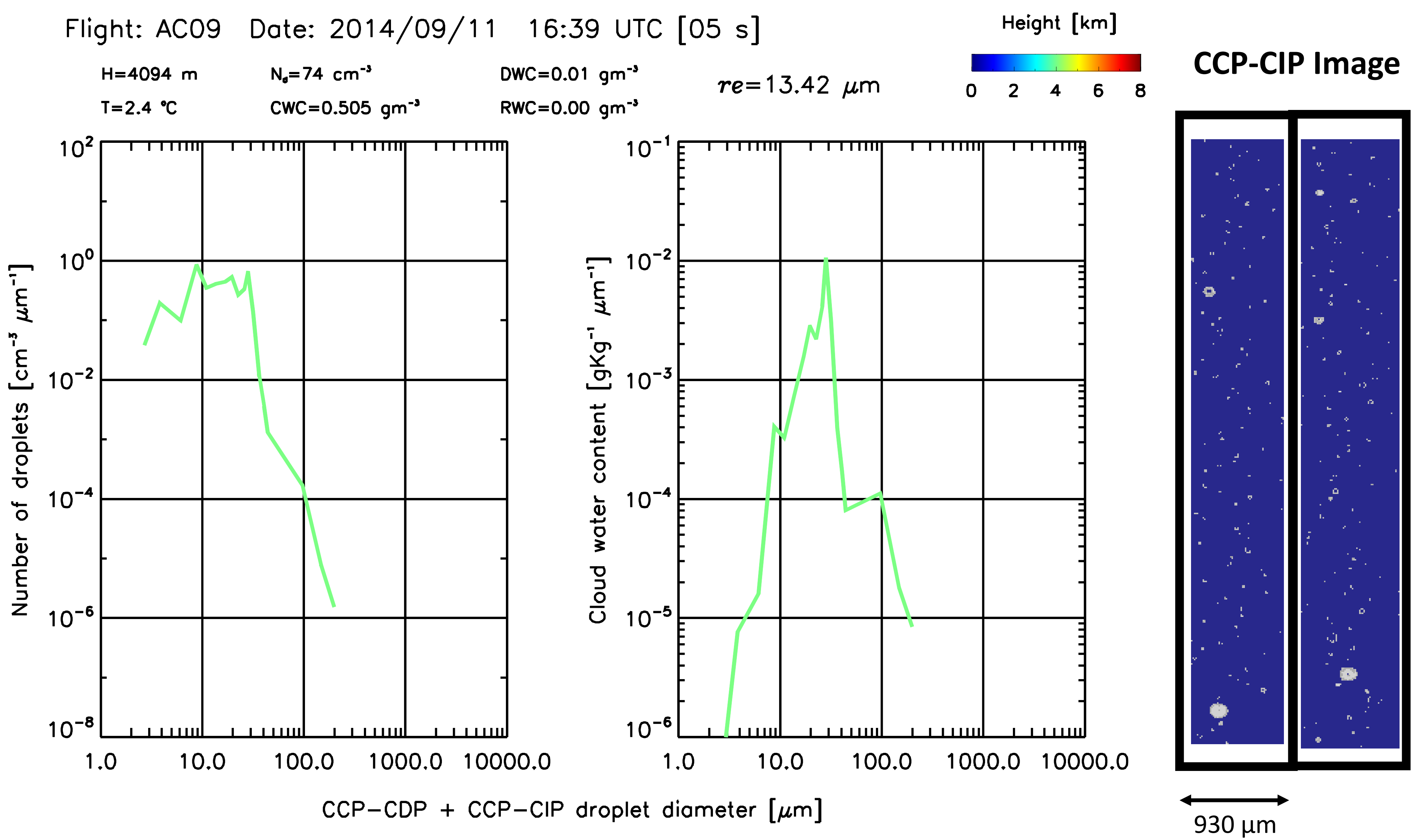

Flight: AC09 Date: 2014/09/11 16:39 UTC [05 s]
H=4094 m
T=2.4 °C
N_d=74 cm⁻³
CWC=0.505 gm⁻³
DWC=0.01 gm⁻³
RWC=0.00 gm⁻³
re=13.42 μm
Height [km]
0 2 4 6 8
CCP-CIP Image
Number of droplets [cm⁻³ μm⁻¹]
Cloud water content [gKg⁻¹ μm⁻¹]
1.0 10.0 100.0 1000.0 10000.0
CCP−CDP + CCP−CIP droplet diameter [μm]
930 μm

b)

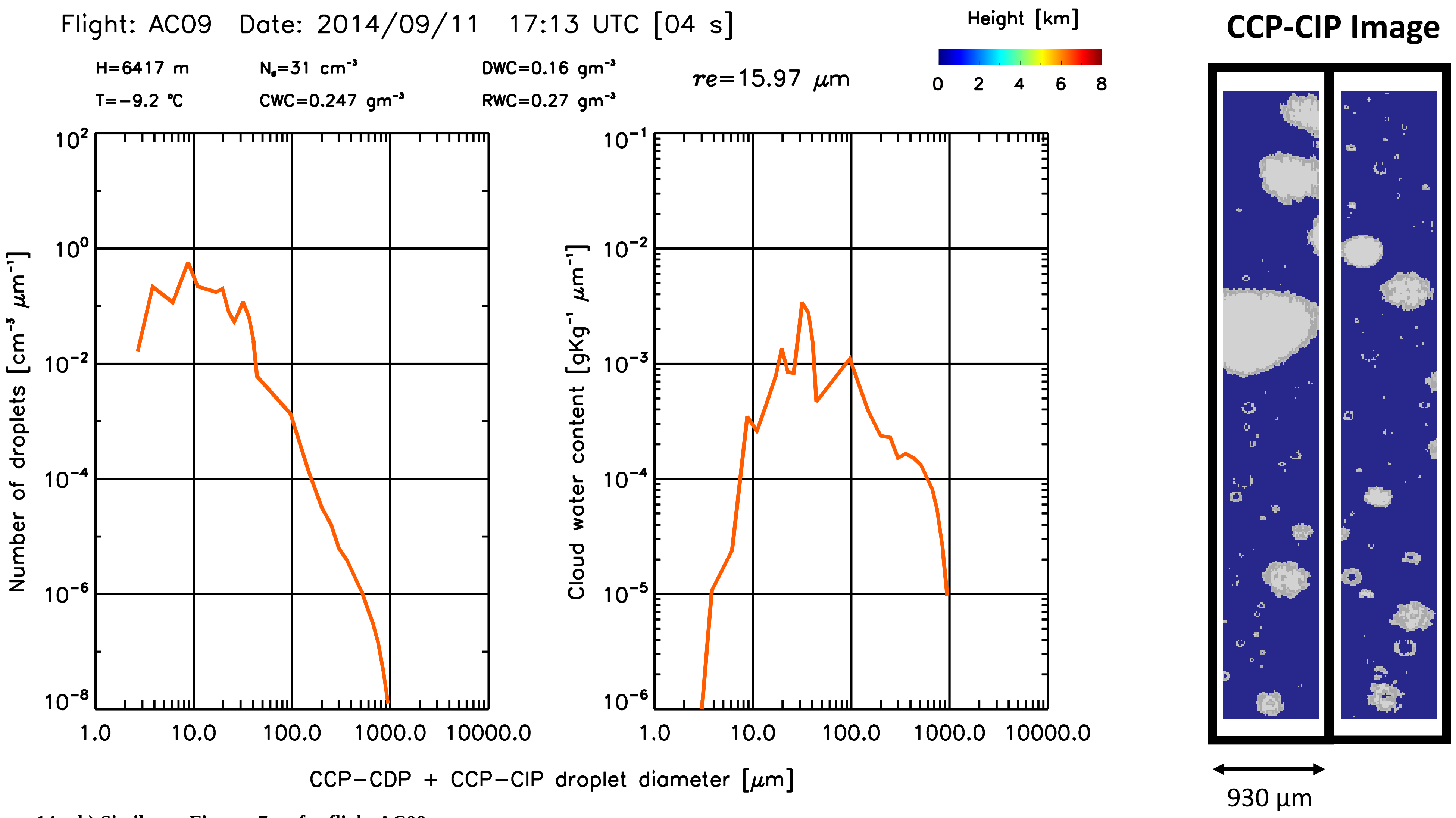

Figures 14 a-b) Similar to Figures 7a-c for flight AC09.

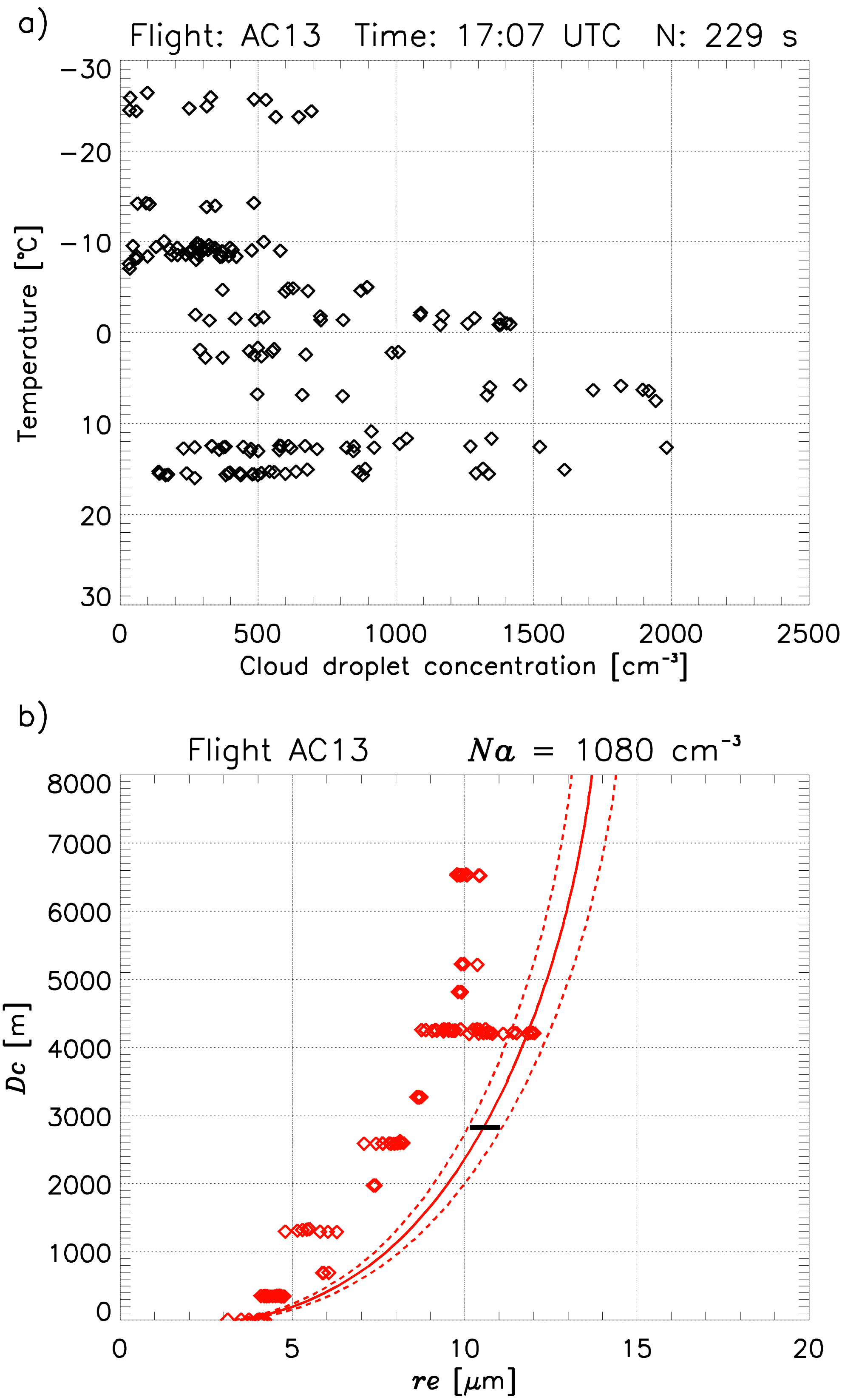

Figure 15 a) Cloud droplet concentration measured with the CCP-CDP probe as a function of temperature for flight AC13. Each dot indicates a 1-Hz average concentration. The sample number and the approximate time of the cloud profile are shown at the top of the panel; b) Similar to figure 9 for Flight AC13.

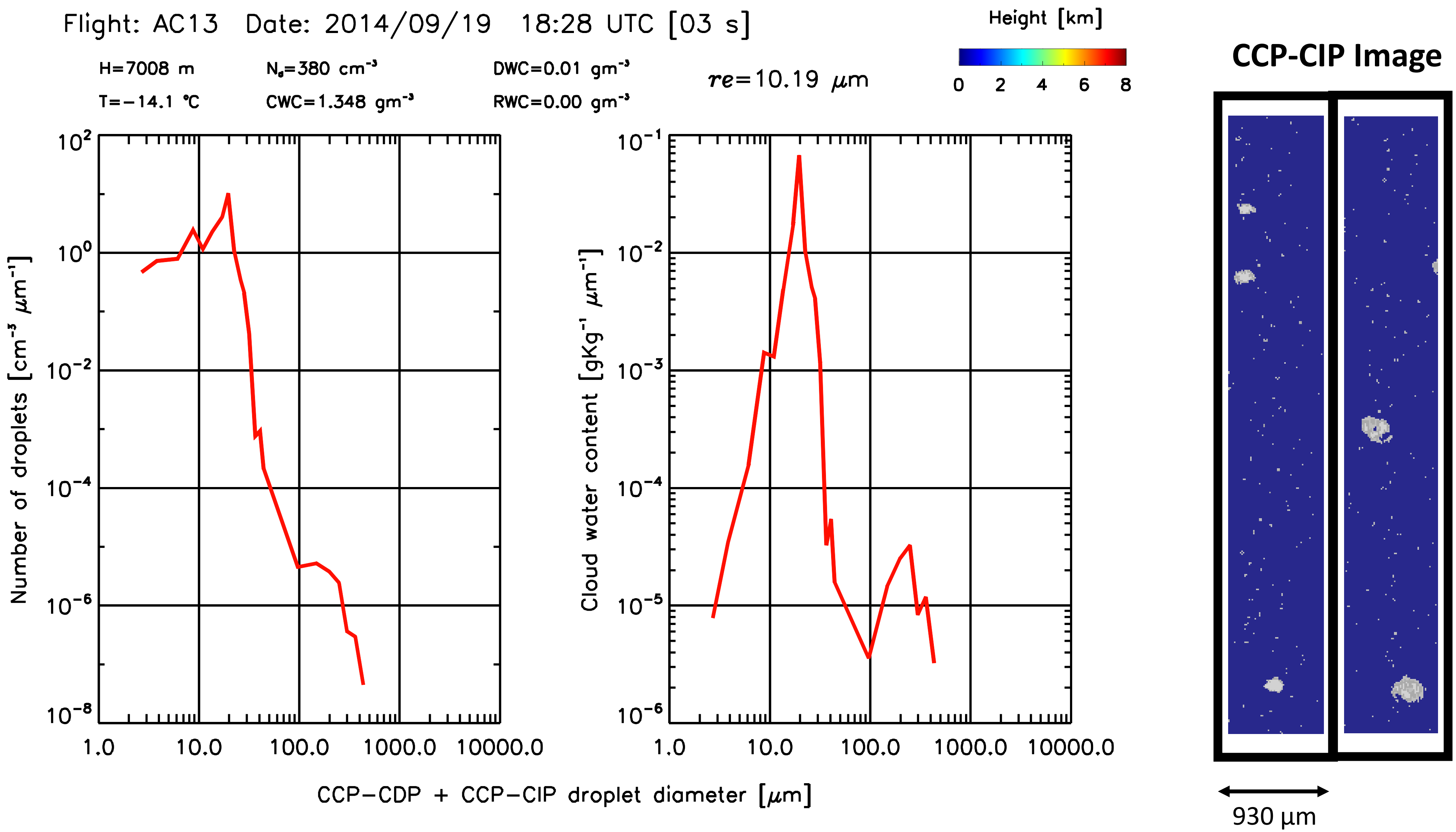

Figures 16 Similar to Figures 7a-c for flight AC13.

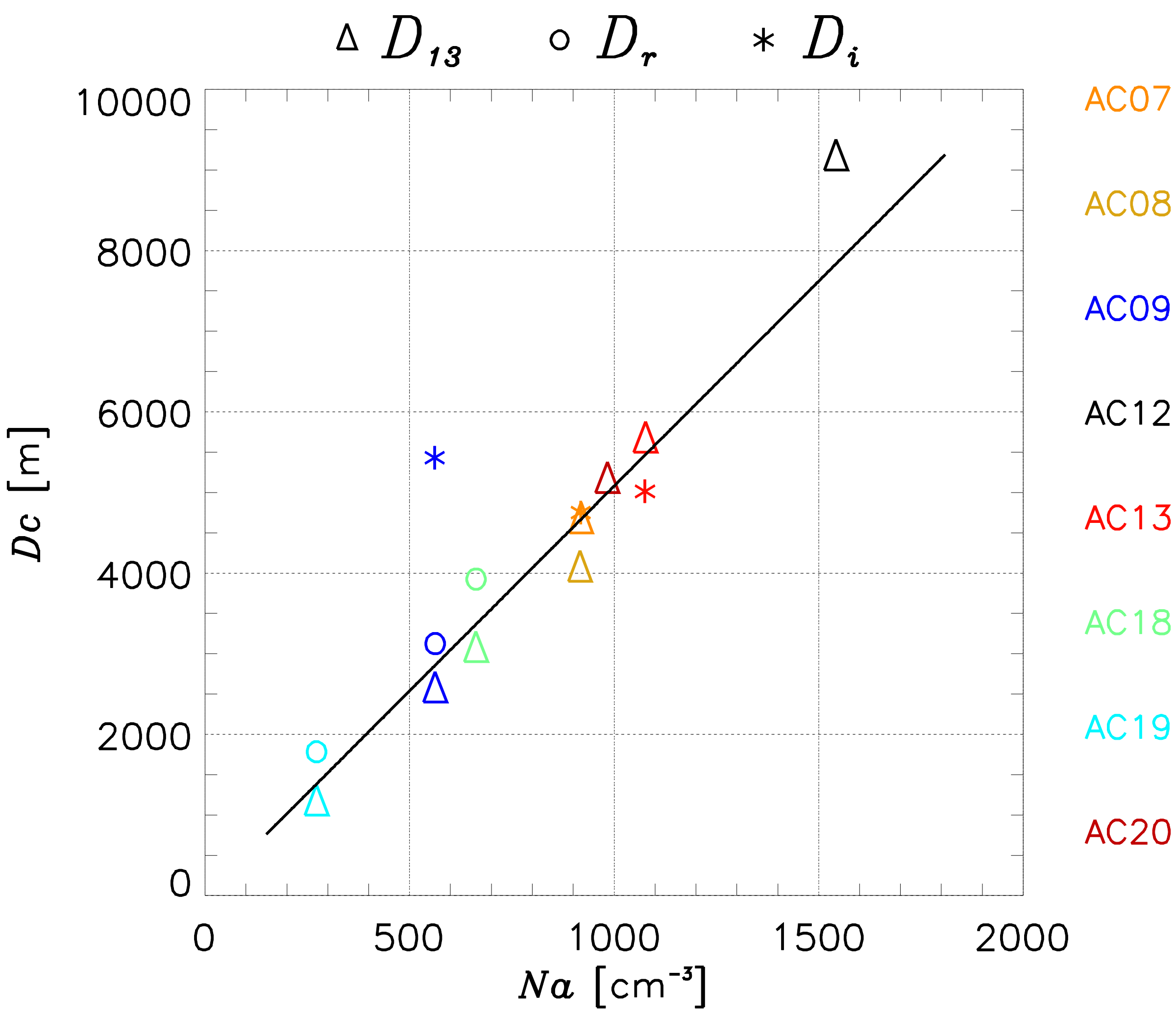

Figure 17 Cloud depth (D_c) as a function of the estimated adiabatic number of droplets (N_a) at cloud base. D_c for adiabatic cloud droplet effective radius (r_{ea}) equal 13 µm (or D_{13}) are indicated by triangles. Similar for cloud depth of rain initiation (D_r) [indicated by circles] and cloud depth for ice initiation (D_i) [indicated by asterisk]. The flight numbers are indicated by colors on the right side of the panel. The values of D_{13}, D_r, and D_i are shown in Table 1. The black line indicates the linear equation for D_{13} as a function of N_a for all flights, where: $D_r = (5\pm0.7)N_a$

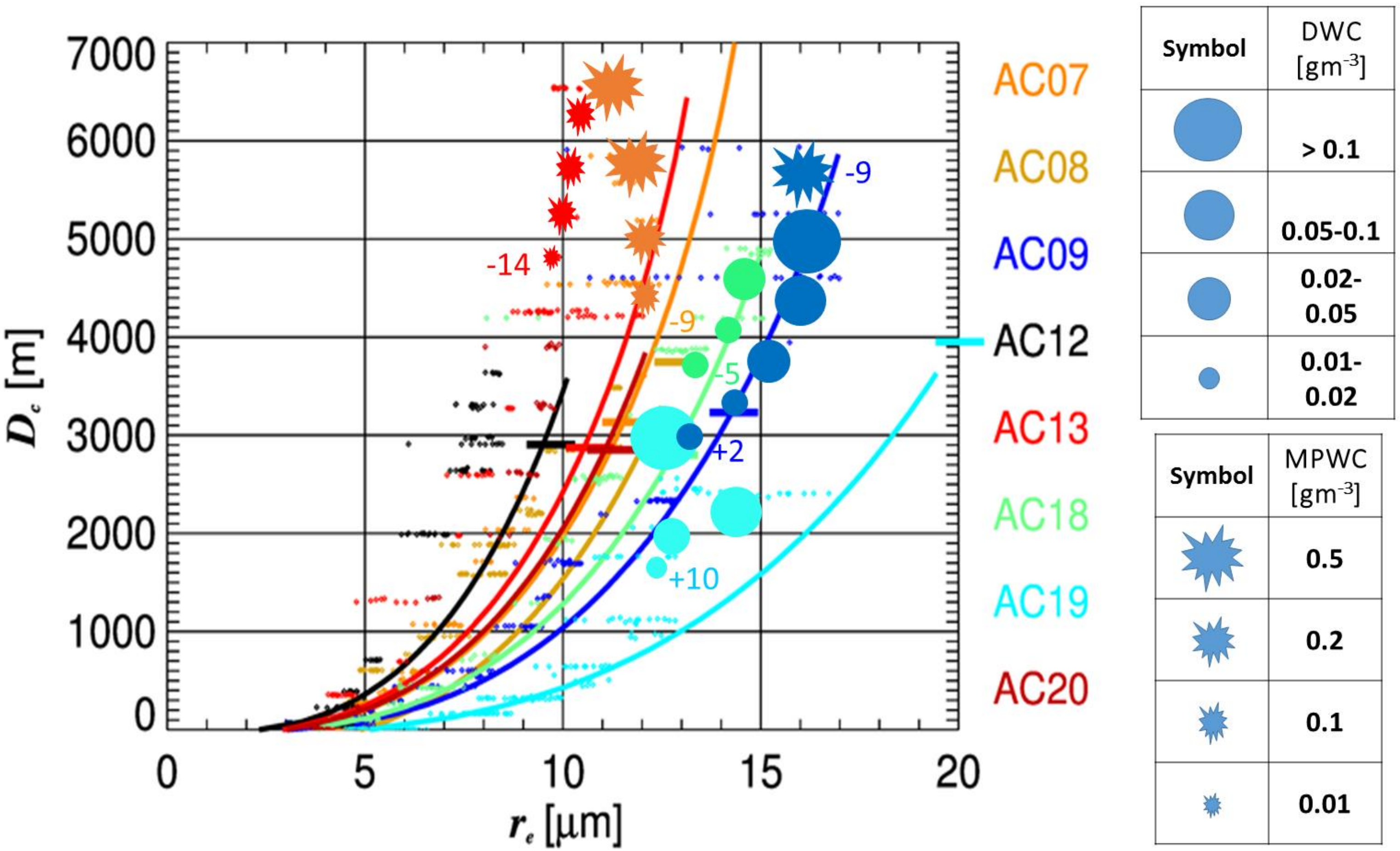

Figure 18 CDP-measured cloud droplet effective radius (r_e) (colored dots) and estimated cloud droplet adiabatic effective radius (r_{ea}) (colored lines) as a function of cloud depth (D_c) for all flights (indicated by colors). The height of 0 ºC is indicated by a horizontal bar across the r_{ea} line. The circles indicate the approximate values of drizzle water content (DWC) calculated from the CCP-CIP data, the range of DWC values is indicated in the table at the upper-right side of the figure. The star symbols indicate approximate mixed phase drizzle water content (MPWC) values calculated from the CCP-CIP data (indicated in the table at the bottom-right side of the figure). The temperature in ºC of rain or ice initiation (D_r and D_i, respectively) is indicated by colored numbers close to the circle or star symbols.